The present work was submitted to the Chair of Space Propulsion and Mobility

presented by

Sven Julius Steinert

Student ID No.: 03773515

Semester Thesis

Design of a Hall Thruster and Investigation for a Water Electrolysis Propulsion System

Munich, March 20, 2024

Supervising professor: Prof. Dr.-Ing. Chiara Manfletti
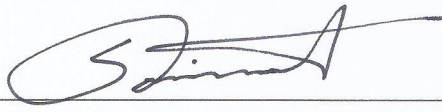Assistant supervisor: Sören Heizmann, M.Sc.

1st   examiner: Prof. Dr.-Ing. Chiara Manfletti

Eidesstattliche Erklärung

Hiermit erkläre ich, dass die vorliegende Arbeit von mir selbstständig verfasst wurde, und dass keine anderen als die angegebenen Hilfsmittel benutzt wurden. Die Stellen der Arbeit, die anderen Werken dem Wortlaut oder Sinn nach entnommen sind, sind in jedem einzelnen Fall unter Angabe der Quelle als Entlehnung kenntlich gemacht. Diese Erklärung erstreckt sich auch auf in der Arbeit enthaltene Grafiken, Zeichnungen, Kartenskizzen und bildliche Darstellungen.

Ich erkläre mich außerdem damit einverstanden, dass meine Master-, Bachlor- oder Semesterarbeit vom Lehrstuhl auf Anfrage fachlich interessierten Personen, auch über eine Bibliothek, zugänglich gemacht wird, und dass darin enthaltene Ergebnisse sowie dabei entstandene Entwicklungen und Programme vom Lehrstuhl für Raumfahrtantriebe und -mobilität uneingeschränkt genutzt werden dürfen. (Rechte an evtl. entstehenden Programmen und Erfindungen müssen im Vorfeld geklärt werden.)

München, 19.03.2024
Ort, Datum

Unterschrift

Name: Sven Julius Steinert
Matrikelnummer: 03773515

Chair of Space Propulsion and Mobility (Prof. Manfletti)
TUM School of Engineering and Design
Technische Universität München

TUM

Semester Thesis

Investigation and design of a Hall Effect Thruster for a Water Electrolysis Propulsion system

Topic

One of the most promising technologies in the ongoing search for high-performance green propellants is the Water Electrolysis Propulsion technology (WEP). The fundamental concept of such a system is to fill the spacecraft on ground with pure water instead of highly toxic propellants. Once the spacecraft is in orbit an electrolyser is used to split up the water into gaseous hydrogen and oxygen. The gases can then be used in a chemical or electrical thruster to propel the spacecraft.

The combination of electrical and chemical thrusters in propulsion system with a common propellant supply is one of the major advantages

Satellite Image Source: www.esa.int/Applications/Telecommunications_Integrated_Applications/Chameleon_satellite_to_revolution se_telecom_market

Figure: Example image of a WEP Satellite

of WEP, as this ability is enabling a unique flexibility. Currently the most suitable electric thruster type for WEP is considered to be a Hall Effect Thruster. Within such a thruster the molecular oxygen is feed to the anode and the molecular hydrogen to the anode. As such thrusters are typically operated with noble gases, various challenges have to be solved before these new propellants can be used reliably and at a competitive performance in such a thruster type.

This thesis shall therefore investigate the thruster behaviour when operated with gaseous O_2/H_2, using various trade-offs and simulations. Based on the simulation results a subsequent initial thruster design shall be derived. Finally, a roadmap for a potential subsequent thruster development shall be evaluated.
(An experimental validation of the magnetic properties can be conducted, if possible with respect to feasibility, time and budget.)

Tasks

- Familiarization with the WEP and Hall Effect Thruster technology
- Literature research on Hall Effect Thruster designs and working principles
- Impact assessment of operation with O2/H2 on thruster behaviour
- Trade-off study to identify the most suitable design principle for an O2/H2 Hall Effect Thruster
- Requirements identification and preliminary dimensioning of relevant design parameters
- Simulation of the magnetic properties, plasma generation and acceleration, as well as thruster performance estimation
- Analysis of simulation results and respective adaptation of design parameters with subsequent design of the Hall Effect Thruster
- Identification and evaluation of a potential subsequent thruster development roadmap
- To be assessed as a function of time and cost: Manufacturing of magnetic subassembly and experimental validation of simulation results
- Documentation and presentation of the results

Contact

Sören Heizmann, M.Sc.
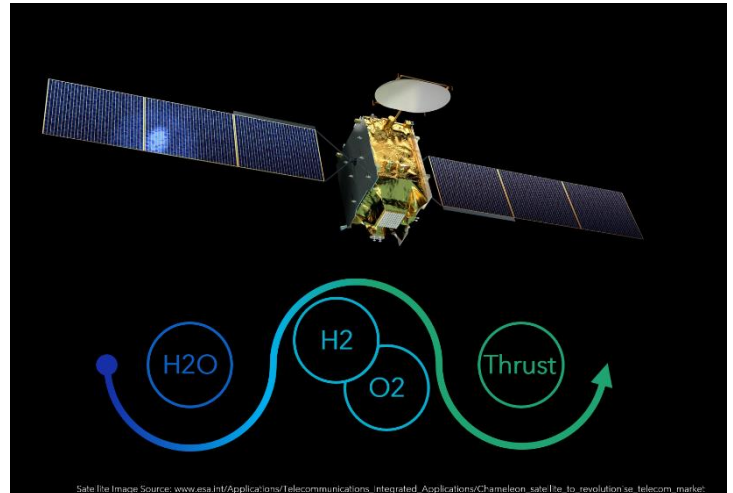+49 89 289 55592
s.heizmann@tum.de

Contents

List of Figures

List of Tables

List of Symbols

General Symbols

$\dot{m}$	[mg/s]	Mass flow
A	$[m^2]$	Surface Area
B	[Tesla]	Magnetic flux
C	[C]	Coefficient (scaling law)
d	[mm]	Mean diameter (discharge channel)
E	[V/m]	Electric Field
F	[N]	Force
g_0	$[m/s^2]$	Standard gravity
H	[A/m]	Magnetic field strength
h	[mm]	Height (discharge channel)
I	[A]	Current
I_{sp}	[s]	Specific impulse
L	[mm]	Length (discharge channel)
L_c	[m]	Characteristic length
m	[kg]	Mass
P	[W]	Power
q	[C]	Charge
R	[Ω]	Resistance
r_g	[m]	Gyroradius (Larmor-radius)
T	[mN]	Thrust
t	[s]	Time
U	[V]	Voltage
v	[m/s]	Velocity

Greek Symbols

α	$[K^{-1}]$	Temperature coefficient
β	[-]	Fitting coefficient
η	[-]	Efficiency
ω_g	[Hz]	Gyrofrequency (cyclotron frequency)
ρ	$[\Omega \cdot mm^2/m]$	Resistivity

Subscripts

$[\ ]_\perp$	Perpendicular
$[\ ]_a$	Anode
$[\ ]_B$	Magnetic field
$[\ ]_c$	Cathode
$[\ ]_d$	Discharge
$[\ ]_E$	Electric field
$[\ ]_e$	Electron
$[\ ]_i$	Ion
$[\ ]_n$	Neutral
$[\ ]_{opt}$	Optimal
$[\ ]_{Ox}$	Oxygen
$[\ ]_p$	Propellant Utilization
$[\ ]_{sp}$	Specific
$[\ ]_{test}$	Testing range
$[\ ]_T$	Thrust
$[\ ]_{Xe}$	Xenon

1 Introduction

In an upcoming era of increasing accessibility of space, new propulsion methods and propellants could be a rising opportunity. Until now, most spacecraft designs have been driven by optimizing for maximum performance only, regardless of price or considerations for mass production or new synergies from emerging space infrastructure. Through lower launch costs, new markets with new niches emerge, where alternative propellants can compete on factors as cost effectiveness, ease of handling, sustainability, by use of abundant materials, or utilization of in space materials. Water electrolysis propulsion (WEP) is one alternative propulsion method that engages all of the mentioned factors through the use of water as abundant, cheap, non-toxic, dense and yet still potent propellant when electrolyzed. The core idea of WEP is to effectively use water as energy storage from solar generated electric power and release it for thrust in a combustion of the produced Oxygen and Hydrogen. This work is about complementing that setup with a low thrust high efficiency stage through electric propulsion to make a WEP system capable to generate both, high thrust, low burn time maneuvers, as well as long time, low thrust but high delta-v maneuvers.

This investigation starts by comparing available electric propulsion methods and evaluating their usability on WEP, as well as experimental ideas on how ions can be extracted from water, to an estimation of a reasonable power design point for a thruster to suit an application market. From there on, a propulsion method was selected and Hall Thrusters and their functionality, design laws, plasma simulations and experimental reference data are analyzed in detail leading into a full design specification of a Hall Thruster running on Oxygen on a comparable power point.

This work is laying the foundation of research on electric propulsion at the chair of Space Propulsion and Mobility at the Technical University of Munich and proposes a road map on implementation of the designed thruster and required infrastructure.

2 Water Electrolysis Propulsion

In this chapter, the background is given under which the thruster in this work is embedded in the existing research at the universities chair and its general definition of use case is given.

2.1 Concept

Water Electrolysis Propulsion (WEP) is describing the principle to launch a spacecraft loaded with water instead of combustible propellant into space and to create then the propellant components by electrolysis in space. This composes additional challenges, as for example solar power is needed, but also advantages in the propellant handling as water in its liquid form is binding the two propellant components chemically safe and very dense without the need for high pressures or cryogenic temperatures. When compared to a classical bi-propellant or mono-propellant propulsion system, especially the propellant handling is simplified drastically, as water is neither toxic, nor unstable under room temperature and atmospheric pressure. Especially for smaller spacecrafts or mass-manufactured spacecrafts, a simplified handling process makes a great difference together with its cheap price. On the down side, WEP systems can not deliver their full thrust capacity instantaneous without having the electrical power to produce the required Hydrogen and Oxygen mass flow just in time, or to have a significant pre-production phase, where the fuel components are buffered into tanks. However, especially with coasting phases or orbit maintenance this refill time is often present and can be designed into the mission. Long term, the benefit of abundance on water in the solar system could one day enable In-Situ Resource Utilization (ISRU) of water resources in space to refill propellant on other celestial bodies or comets.

The main components of a WEP system are the water tank, the electrolyzer, two buffer tanks for the produced propellants and a chemical thruster.

Electrolyzer

The electrolyzer is the essential system to break up and separate the molecular bond between Hydrogen and Oxygen atoms and therefore converting electrical energy into chemical potential. Conveniently this dissociation of water molecules can be reached by applying an electric potential and conducting a current through the material, a process known as electrolysis. In its most simplest form, the cathode and anode can be submerged into water, separated by a proton exchange membrane (PEM) and under a given current, Oxygen is rising on the anodes surface and Hydrogen on the cathodes surface. This basic principle of gas separation by gravity is used also in earth based industrial applications, however in space, the option of phase separation by gravity is not present, which leads to the need of adaptation on the separation method. Depending on which side of the electrolyzer the water supply is connected, anode feed PEM or cathode feed PEM electrolyzers are classified. One solution to achieve gas separation in space is

the implementation of a cathode feed PEM electrolyzer with an additional water feed barrier, which frees up the cathode of its submerged state, and both the anode and cathode can gas out into open chambers. The water feed barrier hereby supplies just the right amount of water into the cathode chamber in the same rate as the water is getting used up. At the chair of space propulsion and mobility (SPM) at TUM, such an implementation of a cathode feed PEM electrolyzer is the current state of research [13].

Chemical Thruster

When the buffered gaseous Oxygen and Hydrogen are chemically combusted to produce thrust, the theoretical achievable $I_{sp} \approx 400\ s$ under stoichiometric ratio is still among the highest for chemical propellants due to the propellant combination. Such a miniaturized thruster the context of a water electrolysis demonstrator is also content of active development at the chair of SPM at TUM, where the demonstrating 3D printed thruster was designed for 2 N and has started to undergo testing.

Electric Propulsion

An expansion to the concept of WEP is the utilization of electric propulsion. In a hybrid configuration it enables the spacecraft the benefits of high thrust, short burn times of the chemical thruster, as well as low thrust, high I_{sp} maneuvers by the electric thruster. In this configuration, either Hydrogen or Oxygen can be ionized and accelerated in an electric propulsion stage. Hereby is the large mass fraction of water present in Oxygen (89 %) and the smaller fraction in Hydrogen (11 %). This makes Oxygen the preferably used element for the electric propulsion system in WEP. This electric propulsion component is, where this work connects to design an electric propulsion system to expand the research on WEP systems at the universities chair. In the further sections, the electric propulsion segment will be the matter of subject.

Adaptations

Alternatively to water electrolysis, water can also be used directly as input to a Hall Thruster, which mitigates the need for an electrolyzer, as in AquaHET [2]. To operate propulsion on water without an electrolyzer will be called adapted WEP in the further text.

2.2 Existing Solutions

Oxygen as propellant was also previously investigated without the context of WEP back in 2003 at the university of Tokyo [24], where they tested the difference in performance in a Hall Thruster between Xenon and Oxygen. More recent experiments and developments have been done in the context of WEP at the Imperial College London in collaboration with Ura Thruster with their so called WET-HET [29] [28]. Besides those two research groups, Oxygen is commonly not considered for use as propellant due its chemical re-activeness and its high electron affinity and molecular bonds, which makes it an exotic choice of propellant to work with, with only very limited data in a non-optimized state.

2.3 Propulsion Methods

In order to ensure a well based decision for one specific propulsion method, multiple established methods are investigated on their compatibility to WEP.

Hall Thruster

Hall Thrusters are usually running on high atomic mass inert gas elements, which selects Oxygen as the preferred choice in this method. One strong benefit of Hall Thrusters is, that their operation was already demonstrated on a variety of gases, besides Xenon and Krypton also in Argon, Neon and Nitrogen [23] and many more. This is especially possible, as in the discharge channel of a Hall Thruster essentially everything is dissociated, just under different efficiencies and plasma properties. Hereby is the most important material compatibility the wall material, which is only in light interaction with the plasma in a Hall Thruster. This channel is usually made out of boron nitrite which is chemically resistant to Oxygen, which makes Hall Thrusters compatible with WEP. Additionally, Hall Thrusters are often the current state of the art choice for propulsion systems, as in for example the Lunar Orbital Platform-Gateway[16]. Finally, Hall Thrusters are promising to have a positive efficiency correlation under increasing power levels, which is why high power variants are developed and researched today. This makes Hall Thrusters a versatile choice, chemically compatible, actively researched and most importantly even features 2 reference thrusters on Oxygen.

Gridded Ion Thruster

Gridded ion thrusters are the other major technology to implement ion propulsion. They have been also tested on a range of propellants, as on Xenon, Krypton, Argon and Iodine [9]. They also operate usually on high atomic mass inert gas elements, but face one major problem when tried to be combined with Oxygen. In a gridded ion thruster the propellant is first put in a containment where one side faces a grid where a high voltage accelerates ions which happen to pass through the holes, while the neutrals are being reflected by the grid, to stay inside the thruster until they are ionized. The ionization can be achieved through different methods, but radio frequency ionization is a widely used method, as in the RIT-μX [20]. This results in an exposure of the propellant to the grid material which is usually made out of Carbon, which is not chemically compatible with Oxygen. However, if instead carbon, a different material is used for the grid material as Molybdenum, chemical compatibility could be reached for the price of lower performance.

Plasma Thruster

Pulsed plasma thrusters (PPT) or Magnetoplasmadynamic Thrusters (MPDT) can operate on ablative PTFE, light elements as Hydrogen or Helium, but also on noble gases as Argon and even on water [14] or air [33] and many more. The fundamental difference is, that in a plasma thruster the whole plasma is accelerated through the Lorentz force of a strong magnetic field, and not through an electrostatic field as in a gridded ion thruster. Plasma thrusters are therefore a great option as they feature the highest range of possible propellants, however often at a limited efficiency. They could be applied on WEP by using either Oxygen or Hydrogen. Even though plasma thrusters have good literature on Hydrogen as

propellant, it would only yield a small mass fraction on a WEP system, so that either Oxygen would be the preferred propellant or a mixture of both. For the case of a mixture, a plasma thruster could theoretically also combust the propellants and additionally yield thrust from thermal energy combined with the magnetic acceleration of the plasma. In the case of an adapted WEP system, water could also be used directly as propellant. However, no explicit plasma thruster on Oxygen or advanced development on water exists that could be taken as design reference.

FEEP

In field emission electric propulsion (FEEP), ions are directly extracted from a liquid propellant through enormous high electric fields. The required electric field strength can only be locally achieved, which is performed through a sharp tip where the field intensifies. To bring both the propellant and the electric field to this desired shape, a conducting fluid is taken as propellant e.g. Gallium or Indium which shapes under its surface tension and the influence of the electric field a so called Taylor-Cone [26]. At the tip of this Taylor-Cone either ions only or charged droplets are ejected, which are then accelerated by the electric field, which extracted them from the fluid. Due to the high electric fields, this method is able to achieve the highest values of I_{sp}, which are so high that developments rather aim to reduce I_{sp} in exchange for more thrust. As thrust generation is the weakness of this technology due to the very small mass flows possible on the Taylor-Cone tip before the structure experiences instabilities. This makes this technology with Taylor-Cones non applicable to WEP, as neither Oxygen, nor Hydrogen, nor water are conductive liquids that don't boil off under the vacuum of space.

Experimental Ideas

If it would be possible however to extract ions directly from the water into an acceleration stage, WEP could be greatly simplified. As theoretically ions are already created in the process of electrolysis, but then recombined into molecular Oxygen and molecular Hydrogen, great savings on efficiency could be achieved. Due to the fact that additional energy has to be spent to dissociate the molecular bonds, ideally they are not formed in the first place. Possible candidates are Hydronium (H_3O^+) ions and Hydroxide (OH^-) anions, which naturally exist in minor concentration due to autoionization of water. Hydrogen ions (H^+), which are essentially protons are also one possible form of ions to extract from water via electrolysis. In fact, the alkaline cathode reaction is able to produce such Hydroxide anions, and the PEM anode feed reaction is able to create Hydrogen ions. When combined in Equation 2.1, such an electrolyzer would be able to create both, Oxygen and Hydrogen gas, as well as anions and protons which could be both accelerated while still neutralizing each other after they left the electric thruster.

$$
\begin{aligned}
\text{cathode} \quad 4H_2O \xrightarrow{+4e^-} \quad 2H_2 + 4OH^- \\
\text{anode} \quad 2H_2O \xrightarrow{-4e^-} \quad O_2 + 4H^+
\end{aligned}
\tag{2.1}
$$
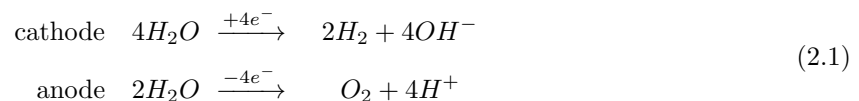
The difficulty would be here to extract the anions and protons. If however accomplished, both charged particles can be accelerated electrostatically, to achieve a most compact WEP setup. A conceptual sketch of this idea is illustrated in Figure 2.1.
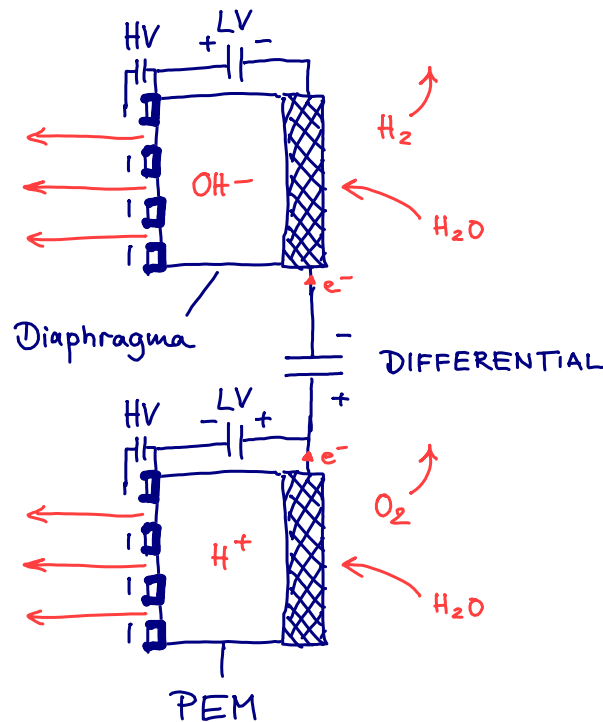
Figure 2.1: Conceptual idea of an aion-proton-electrolysing-thruster which operates under low voltage (LV) and a differential voltage for electrolysis and high voltage (HV) for electrostatic acceleration

Decision

The electric propulsion method chosen for this work is a Hall Thruster, due to the reason that it already has a high technology readiness level and that it was already demonstrated on Oxygen, even in the context of WEP, which gives it an edge over all other methods. Due to the available reference data, lessons learned can be applied and their results can be either tried to be reproduced or taken as baseline for concepts of improvement.

2.4 Application Market

To identify a power design point, the application market is analysed for reference thrusters used in current and upcoming developments for commercial applications. In table 2.1 a number of electric propulsion platforms are listed with their used thrusters, published in a presentation by the European Space Agency (ESA). Hereby is the application market telecommunication satellites in the geostationary orbit. This table is listed from flight proven at the top to under development on the bottom, where a clear trend of increasing power levels of the used thrusters can be identified. Additionally, the latest featured PPS-5000, which besides being able to be throttled on half its power demand, is focused to operate on 5000 W. This power point which is used by multiple contractors gives a clear indication on the currently considered power level for today's developments.

Platform	Prime Contractor	Status	EP Thruster	unit Power*	EP Type
ARTEMIS	Thales Alenia Space Italy	Flight Proven	2× UK-10 (T5)	658 W	GIE
			2× RIT-10	760 W	
Eurostar E3000	Astrium	Flight Proven	4× SPT-100	1350 W	HET
SpaceBus	Thales Alenia Space	Flight Ready	4× PPS-1350G	1500 W	HET
AlphaBus	Astrium / Thales	Flight Proven	4× PPS-1350G	1500 W	HET
AlphaBus Extension	Astrium / Thales	Flight Proven	4× PPS-1350G 4× PPS-1350G Option T-6	1500 W	HET /GIE
SGEO	OHB	PFM 2014	8× SPT-100 or 8× HEMPT	1350 W	HET
NEOSAT	Airbus / Thales	Under Development	4× PPS-5000	2500 W - 5000 W	HET
ELECTRA	OHB	Under Development	4× PPS-5000	2500 W - 5000 W	HET

Table 2.1: Reference platforms with their electric propulsion (EP) system and used thrusters (from ESA presentation [8]) and their power per unit (* separately looked up)

As later in ESA's presentation concluded, the 5 kW power level for the telecommunication market is where a commercial competitive power point lies, which is why this is taken as market reference for the upcoming years, with tendency to increase in power.

However, due to the fact that the reference Hall Thrusters on Oxygen have been operated on lower power levels than 5 kW, the power point for the designed thruster is adapted to be both comparable to the reference thrusters while still not being to far away from the target of a commercial 5 kW power point. The Oxygen Hall Thruster tested at Tokyo university was operated at 1 kw [24], while the WET-HET at the Imperial Collage London was tested in a wide range from around 80 W to 2238 W [34].

This leads to the decision to design the thruster on 1 kW, so that data from both thrusters can be used during the design phase and later during testing to compare results. As this is being the first developed electric propulsion system at the Technical University of Munich, the lower power level could be advantageous on the infrastructure requirements, to simplify implementation while still being able to conduct research and gaining experience and insight on an experimental demonstrator.

3 Hall Thruster Design

Historically, Hall Thrusters have already been developed long ago by the Soviet Union, dating back in the 1960s and later also by the United States. As different propulsion methods have been explored, especially the soviet Stationary Plasma Thruster (SPT) series of Hall Thrusters had the most considerable impact and a very long flight heritage. The SPT series exists in many sizes and variants as adopted on many power levels and improvements over time have been introduced. The first one ever launched was an SPT-50, which was launched in 1971 on the soviet Meteor satellite and today, hundreds of Hall Thrusters are currently operating in orbit. One state of the art usage is the fleet of the starlink constellation satellites, as they are equipped with Krypton fueled Hall Thrusters [32]. But also by agencies Hall Thrusters are used as primary propulsion, as in ESAs SMART-1 mission [18] or NASAs Psyche mission [31]. Besides the 1.35kW class SPT-100 [5] which was excessively tested and is often taken as historical baseline, more modern developments are the 1.5kW class PPS-1350 by Safran [25] or for the Hall Effect Rocket with Magnetic Shielding (HERMeS) at the Jet Propulsion Laboratory (JPL) for the upcoming Advanced Electric Prolusion System (AEPS) on the Lunar Gateway which will operate on 12 kW [16]. Common numbers of these Thrusters are shown in Table 3.1. Current developments opt to achieve higher lifetimes by mitigating erosion and especially work on proceedings in higher power levels than ever before.

variable	unit	SPT-100	PPS-1350-S	HERMeS
P	W	1350	1500	12000
U	V	300	350	600
$\dot{m}$	mg/s	5.0	5.5*	22.1*
I_{sp}	s	1600	1660	2826
T	mN	80	90	612.9
η_T	%	50	50	67.2
propellant	-	Xenon	Xenon	Xenon

Table 3.1: Common numbers of famous Hall Thrusters based on [5],[25],[16] (* from context)

3.1 Working Principle

The major components which make up a Hall Thruster (illustrated in Figure 3.1) are the discharge channel, the anode, the cathode, and the magnetic body with coils. The discharge channel is where neutral propellant is injected, which is then ionized by electrons and accelerated out of the thruster. The anode is the electrical positive end and at the same time the propellant inlet, where neutrals enter the discharge channel. The cathode is the electrical negative which is an electron emitting source, which is either placed in the center or attached to the side of the thruster, so that the electrons can enter the discharge channel from the outside of the thruster. The magnetic body and coils are creating a magnetic field which plays a crucial role into trapping electrons inside the discharge channel near the exit plane.
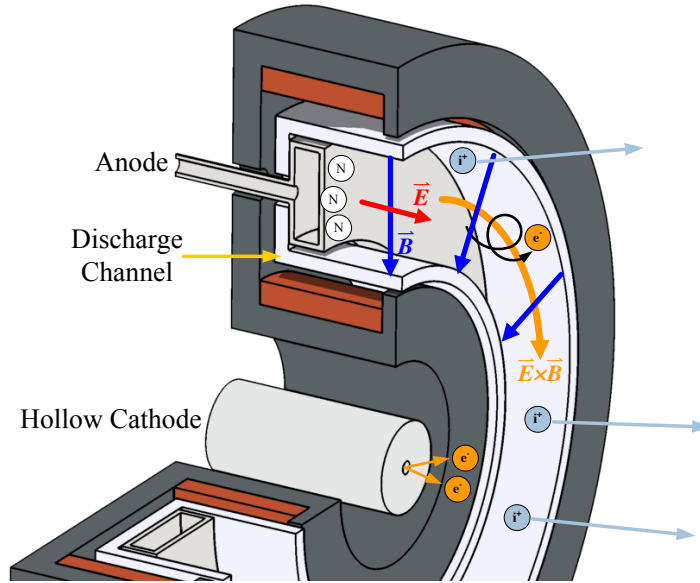
Figure 3.1: *"Hall-effect thruster schematic"* - Raymond Liang [21]

Unlike its name suggests, there is actually no classical Hall Effect present in a Hall Thruster, but the azimuthal movement of the trapped electrons (ExB in Figure 3.1) is referred to as Hall current. This trapping of electrons is reached by the strong radial magnetic field B which causes the electrons to be magnetised, leading to an ExB drift, which is later described in more detail. A charged entity is called magnetised, when the B field is strong enough to cause a continuous cyclotron movement without the entity leaving the influence of the B field. The cyclotron or gyration radius is more precisely known as Larmor-Radius, which in a homogeneous magnetic field under its perpendicular velocity $v_\perp$ is defined as:

$$r_g = \frac{m \cdot v_\perp}{|q| \cdot B} \tag{3.1}$$

The cyclotron frequency is further defined as:

$$\omega_g = \frac{|q| \cdot B}{2\pi \cdot m} \tag{3.2}$$

This relationship illustrates differences in the Larmor-Radius and cyclotron frequency especially for different masses for ions ($m \approx 10^{-26} kg$) and electrons ($m \approx 10^{-31} kg$) and their state of magnetisation. In a Hall Thruster, the electrons are aimed to be magnetised, while the ions are explicitly not to be magnetised, as the ions ideally only experience the electric field and accelerate straight through the exit plane. The magnetisation of the electrons is essential for their confinement, which from their perspective aims to make the B field as high as possible. This leads to the major design condition of the strength of the B field, which puts the radii into relationship to the characteristic scale length L_c of the thruster:

$$r_{g,e} << L_c << r_{g,i} \tag{3.3}$$

ExB Drift

To understand the ExB drift movement better, the movement of single charged particles is first inspected. The resulting force on a charged particle which moves through an electromagnetic field is called Lorentz force (Equation 3.4), which consists of the sum of the electric and magnetic vectorial force components.

$$F = F_E + F_B = (q \cdot E) + (q \cdot v \times B) \tag{3.4}$$

From that force and a given mass, the acceleration can be derived through $F = m \cdot a$, which can be transferred into a position over time via time step integration which is handled in the created simulation by explicit 4th order runge kutta.

The different movements of electrons and ions are shown in Figure 3.2 for different initial velocities v_0. Hereby the intensity of the electric and magnetic fields are chosen to roughly match conditions in a Hall Thruster. The section where the plotted plane would be located in a Hall Thruster can be seen on the top left corner.
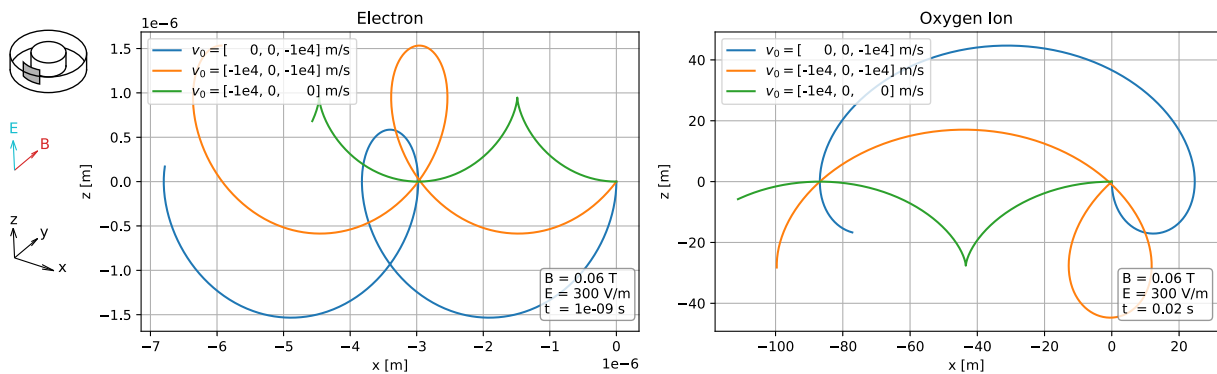
Figure 3.2: ExB drift for electrons (left) and Oxygen ions (right) at different initial velocities v_0

Notably, for one species, all trajectories cross over at exactly one period, which is explained by a constant speed of the guiding center, because the ExB drift velocity is non-dependent on the initial velocity, which can also be seen in the cyclotron frequency of Equation 3.2, which only depends on q, B, m and not on v_0. Furthermore a non-obvious result is the identical drift direction for both positive and negative charges, which however, does not play a significant role in a Hall Thruster.

What on the other hand is relevant for a Hall Thruster, is that this ExB drift is dominantly present for electrons but not for the ions, which comes again down to the condition of Equation 3.3, that the exposed length is big enough to magnetise and drift the electrons but not the ions. This can be seen in the units of Figure 3.2, that for a discharge channel in order of mm, the electrons movement is in the order of μm and the ions in the order of m.

This means that for a scale of mm, the ions travel unchanged with their initial velocity v_0, which results in the ions being able to cross the magnetic field in the discharge channel essentially without any disturbance. For the electrons however, a magnetic influence in the order of mm is magnitudes higher than their cyclotron radius, which results into a ExB drift dominated movement, which most importantly prevents the electrons from traveling into the direction of the electric field and thus to the anode. This

means that a flow of incoming electrons is diverted into an eternal ExB drift movement perpendicular to the anode, which is only diverted through collisions which can resolve their trapped state. In a Hall Thruster this is the key to its functionality, as these collisions can cause ionization of the propellant but also the collective mass of trapped electrons expel a strong electric field as space charge which accelerates the created ions right at their point of creation.
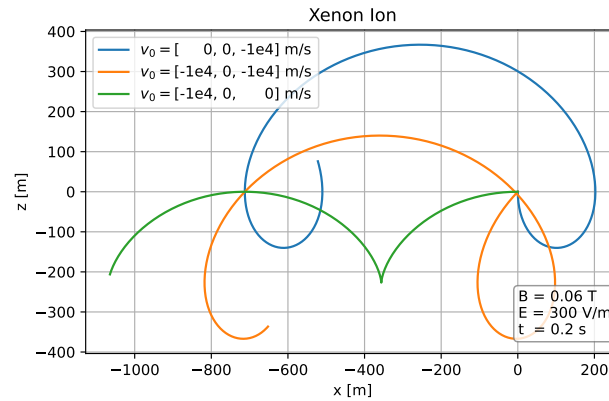
Figure 3.3: ExB drift for Xenon ions at different initial velocities v_0

When the cyclotron movement of Oxygen ions is compared to Xenon ions in Figure 3.3, the Xenon ions have roughly one magnitude bigger scales, which can be explained by the difference in atomic mass units from 15.999 u (Oxygen) to 131.293 u (Xenon) also being roughly one magnitude apart (offset of subtractive electron mass neglected due to insignificance). This results in a decrease in the upper limit of roughly one magnitude for the condition in Equation 3.3, when switching from a Xenon design to one for Oxygen. However, this would only become a problem if the characteristic length of the thruster, hence its magnetic region of the discharge channel, or more conservative the thruster geometrics approach sizes in meters rather than millimeters.

Trapping in Discharge Channel

This understanding is now transferred into a 3D simulation of electron movement to be closer to an actual discharge channel. Unlike the 2D simulation, this can implement a truly radial B field with movements of azimuthal components. It showed, that only a radial magnetic field is not enough to achieve the electrons moving azimuthal around the thruster. For this, an additional effect has to be considered.

When many electrons are placed around the thruster in the discharge channel, the first local change of direction by the ExB drift causes all of the electrons to drift first tangential to the discharge channel. This initial stream of electrons is essentially an electric current, which is inducing a magnetic field itself that effects other electrons. The result of these two overlapping magnetic fields is a vectorial sum of both fields. A cross section of the magnetic field in the discharge channel is shown in Figure 3.4, with the radial component induced by the magnetic coils, together with the hall current induced magnetic field, as well as the resulting sum of both influences.
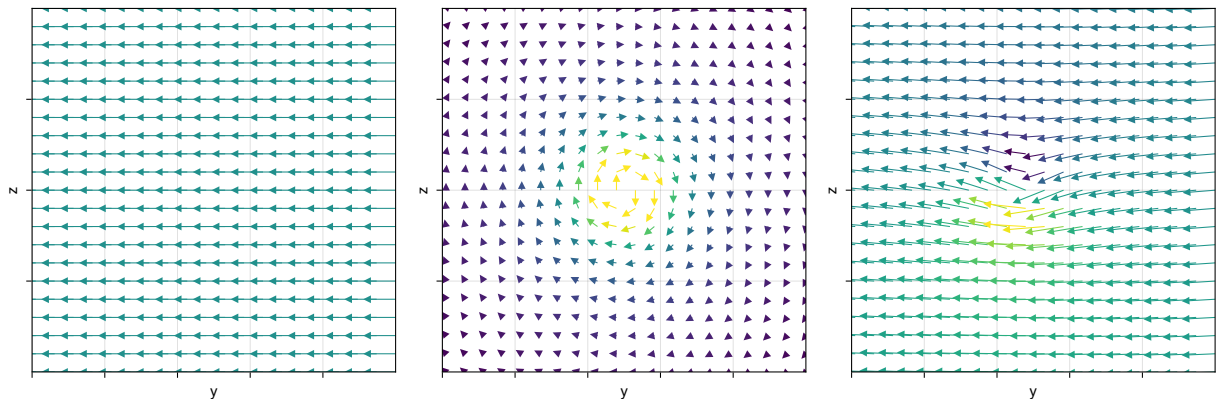
Figure 3.4: Magnetic field: radial (left), hall current induced (center) and resulting sum (right)
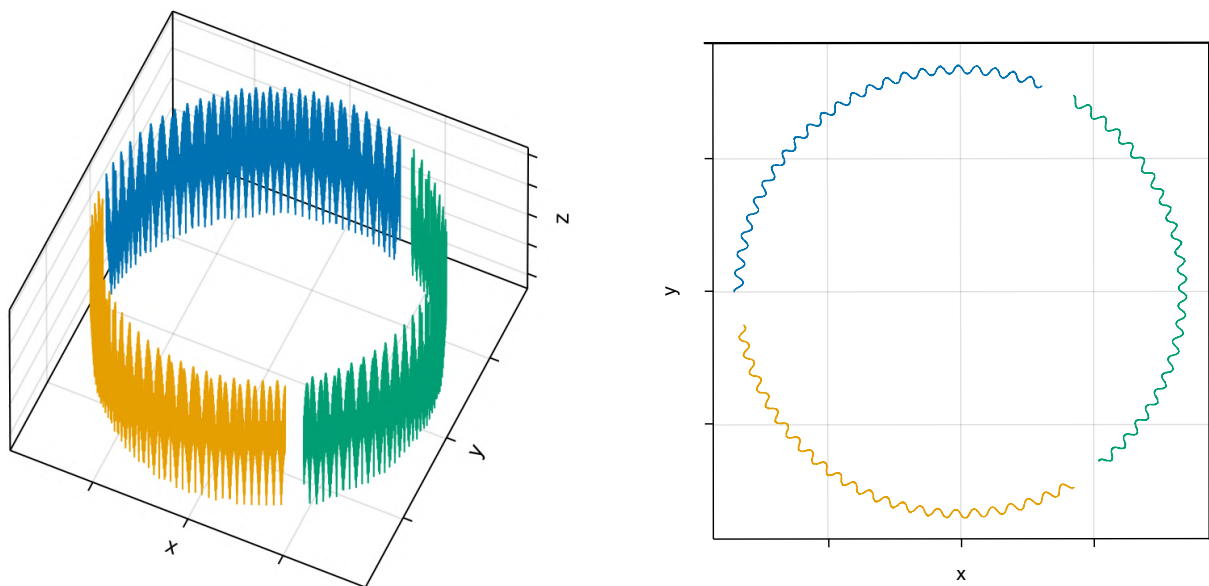
Figure 3.5: Trajectory of 3 electrons in the combined magnetic field showing perfect confinement around the discharge channel

When the numerical electron simulation from earlier in applied on this 3D magnetic field with the hall current component, perfect confinement can be observed as plotted in Figure 3.5. In reality however, this confinement is far from perfect and the electrons collide not only with other electrons but also with the wall of the discharge camber regularly, which makes this plotted path of an electron a great simplification to understand the basic principle of confinement, but not a realistic simulation of the plasma.

Electrons Energy Distribution

One important concept for plasma interactions is the thermic distribution of electrons. It describes, that under a specified temperature, usually measured in electron volts (eV), the energy of a single electron is distributed by a Maxwellian-Boltzman-Distribution. In this context, the energy state of a single electron is directly its kinetic energy and therefore can be translated to its velocity, as this elementary particle has no modes of oscillation as for example molecules have. As a consequence, the amount of electrons to undergo a specific reaction or the specific path they are taking is described through a probability.

Sequence of Ionization

The fundamental difference between Xenon and Oxygen as propellant is the sequence of ionization. In the case of Xenon or any noble gas, there is only one reaction required to form the desired ions. As Xenon is already present in atomized form, an electron collision with sufficient energy can perform ionization as in Equation 3.5. The minimum energy spent per Xenon ion is its first ionization energy 1170.4 kJ/mol.

$$\text{Xe} + e^- \rightarrow \quad \text{Xe}^+ + 2e^- \tag{3.5}$$

For the Oxygen molecule however, the minimum reaction to achieve ions is a chain of dissociation to ionization as in Equation 3.6. This results in the minimum energy spent per Oxygen ion to be its first ionization energy 1313.9 kJ/mol plus half the molecules dissociation energy of 498.34 kJ/mol, as two Oxygen atoms are freed, resulting in 1563.07 kJ/mol per Oxygen ion.

$$\begin{aligned} \text{O}_2 + e^- &\rightarrow \quad 2\,\text{O} + e^- \\ \text{O} + e^- &\rightarrow \quad \text{O}^+ + 2e^- \end{aligned} \tag{3.6}$$

This difference in minimum energy spent per ion amplifies, when translated to thrust T and thrust efficiencies η_T, because of the fact that the Xenon ions have a much greater mass than the Oxygen ions under identical charge. This becomes present when compared at an identical I_{sp} where both ions have the same velocity but the Xenon has the higher impulse, as $T = m \cdot I_{sp} \cdot g_0$. This higher impulse can also be matched with simply more Oxygen ions, however this also increases the amount of energy spent on dissociation and ionization.

When analyzed on thrust efficiency η_T where the kinetic energy E_{kin} is the desired parameter and ionization and dissociation energies are seen as losses E_{loss}, the maximum achievable efficiency is then dependent on I_{sp} as in Equation 3.7 with minimal losses to be $E_{loss} = 1170.4\ kJ/mol$ for Xenon and $E_{loss} = 1563.07\ kJ/mol$ for Oxygen. In Figure 3.6 this is plotted for a range of I_{sp}.

$$\eta_T(I_{sp}) = \frac{E_{kin}}{E_{kin} + E_{loss}} = \left(\frac{m}{2} \cdot \left[I_{sp} \cdot g_0\right]^2 \right) \div \left(\frac{m}{2} \cdot \left[I_{sp} \cdot g_0\right]^2 + E_{loss} \right) \tag{3.7}$$
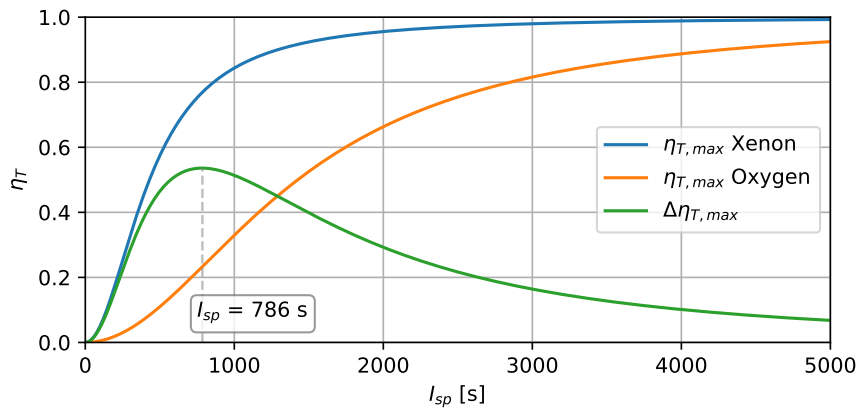
Figure 3.6: Theoretical maximum achievable thrust efficiency dependent on specific Impulse for Xenon and Oxygen and the difference between them

This is the reason why Oxygen is fundamentally disadvantaged to Xenon even under theoretical ideal conditions without any side reactions. Without the simplification of no side reactions and a 100% reaction probability, the characteristics of these curves will deviate from Figure 3.6, so that the illustrated maximum difference should not be taken too serious. As a general trend however, an increase of I_{sp} always increases the absolute number of the thrust efficiency. This way, when thrust efficiencies are being compared, they also need to have a similar level of I_{sp} to be comparable.

Cathode

In order to feed the Hall Thruster with electrons and to neutralize the ejected ions, an electron emitting cathode is required. The emission of electrons can be reached through thermionic emission, where in the simplest case a wire is heated, which lifts the atoms on a higher energetic state, so that under the appliance of a small electric field, electrons can be extracted out of the wire continuously if there is an electrical flow path back to "refill" the electrons. For Hall Thruster cathodes, an emitting material is inserted in a hollow cathode tube als illustrated in Figure 3.7, where a small mass-flow of gas $\dot{m}_c$ protects the delicate emitter material and serves as a plasma medium for the electrons to flow. This emitter material can be Barium Oxide (BaO), Lanthanum Hexaboride (LaB6), Tantalum (Ta) or Yttria (Y2O3).
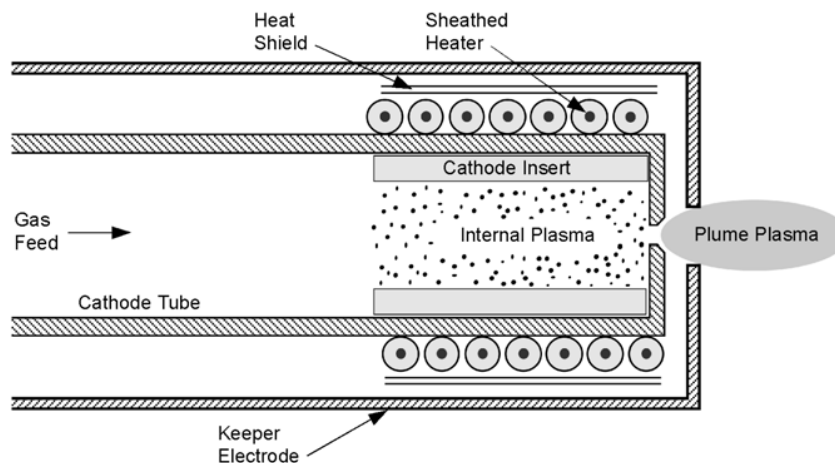
Figure 3.7: *"Hollow cathode schematic showing the cathode tube, insert, and heater enclosed in a keeper electrode."* - Goebel and Katz [11]

As usually the inert gas propellant is also used for the cathode mass-flow, it is not chemically compatible with Oxygen, as this would destroy the emitter material. However, Hydrogen is chemically compatible with LaB6, which could be used in the context of WEP [28]. One difficulty will be the purity of the Hydrogen required to not damage the emitter material.

In an operational configuration, the hollow cathode has multiple internal voltages and one major voltage to the Hall Thrusters anode, over which the discharge voltage U_d will apply. Over this voltage potential the discharge current I_d will flow, which makes up the main power consumption of the Hall Thruster.

3.2 Operating Settings Space

For a given thruster with fixed geometry, materials and magnetic field, the main operational variables are set by only three values: the set discharge voltage, the set anode mass-flow and the set cathode mass-flow.

To better understand how they are connected with the power demand and thrust efficiency, an old data-set from NASA on the SPT-100 is utilized, which contains a great number of tests. To simplify these dependencies, one variable is held static, the cathode mass-flow $\dot{m}_c$ at 0.5 mg/s, while the parameter space of the discharge voltage U_d and anode mass-flow $\dot{m}_a$ is analyzed.

The goal of this analysis is to identify the parameters for optimal efficiency under one level of power. This is reached by first extracting a power iso-line of the variables that can be then be mapped on efficiency.

To achieve interpolation between the data points, a fitting function is used which consists out of higher order polynomials, denoted in Equation 3.8, where β_i are the fitting coefficients.

$$f(x,y) = \beta_0 + \beta_1 \cdot x^2 + \beta_2 \cdot y^2 + \beta_3 \cdot x^2 y + \beta_4 \cdot xy^2 + \beta_5 \cdot x^3 + \beta_6 \cdot y^3 \tag{3.8}$$

First, this fitting is applied on the data-points of U_d and $\dot{m}_a$ against power P. The result of the fitted surface, as well as a power iso-line at 1000 W can be seen in Figure 3.8
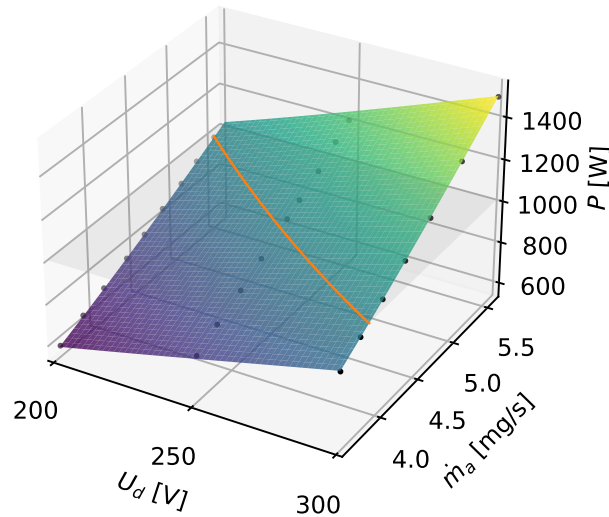
Figure 3.8: Operational parameter space of the SPT-100 data and its fitted surface on power cut horizontally to obtain a power iso-line

The combinations of U_d and $\dot{m}_a$ that result in an equal power demand are plotted in Figure 3.9 on different power levels, together with their derivatives. The characteristics of the power iso-lines only deviate slightly and are mainly a parallel displacement.
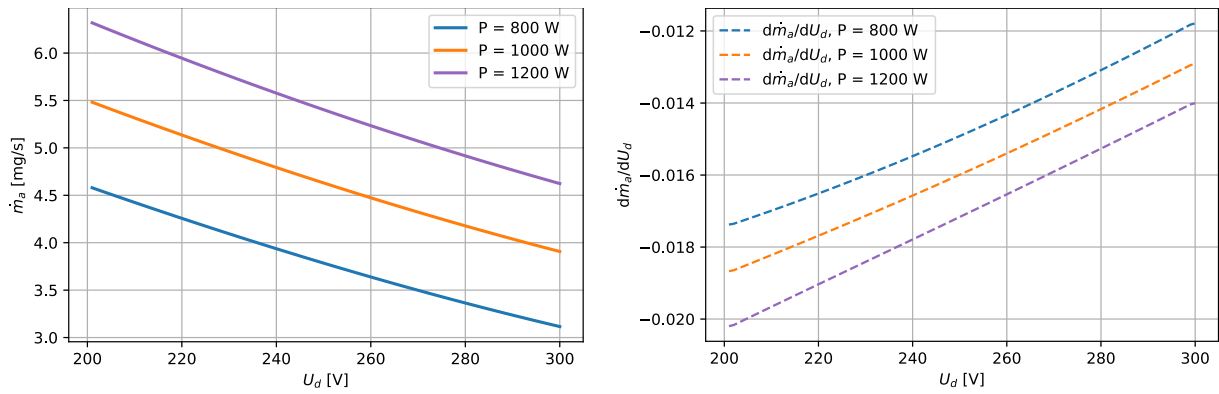
Figure 3.9: Combinations of massflow and voltage that lead to a constant power for different power levels (left) and their derivatives (right)

The data points are fitted again with Equation 3.8, this time on the thrust efficiency η_T, and the power iso-combinations are mapped on the efficiency surface which can be seen in Figure 3.10.
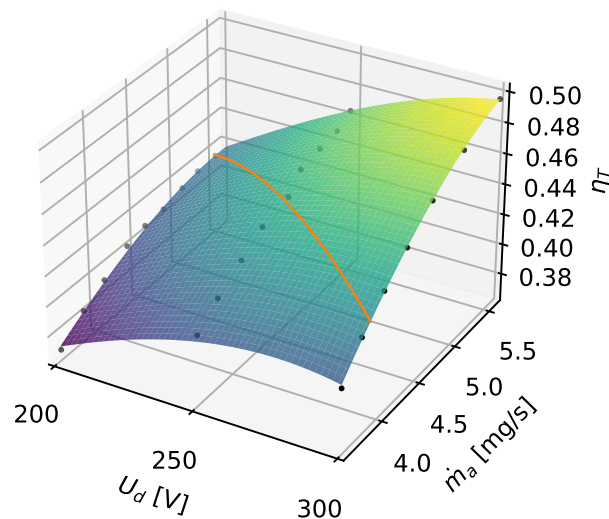
Figure 3.10: Operational parameter space of the SPT-100 data and its fitted surface on efficiency with a projected power iso-line

Figure 3.11 shows the resulting power-iso lines with respect to η_T once for U_d and once for $\dot{m}_a$. It shows, that depending on the power level, there is a distinct optimum for each value of U_d and $\dot{m}_a$. These optimal values are increasing in magnitude with an increasing power level. As this data-set was created by an SPT-100 running on Xenon, the absolute values can not be directly transferred to an Oxygen thruster, as different propellants have vastly different properties, but their characteristics might be similar, so that an analysis like this for Oxygen could end up with only shifted curves. As there is sadly no data set like this available for the Oxygen thrusters, they can only give a reference on how optimal operational settings for one power point can be found.
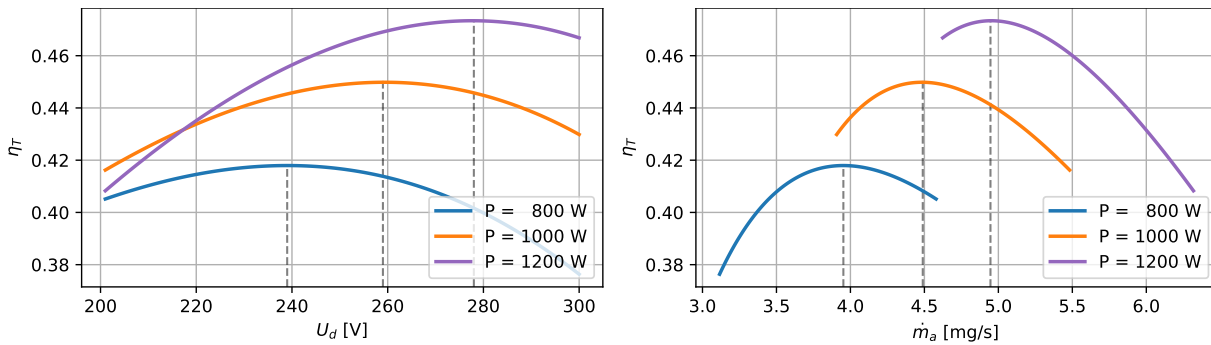
Figure 3.11: Efficiency on a power iso-line over voltage (left) and massflow (right) for different power levels and their combination of maximum efficiency

3.3 Geometric Design

The major design decision of a Hall Thruster comes down to its geometric sizing of the discharge channel. As this volume is the plasma containment and power-densities or surface to volume ratios are determined through it. The geometric parameters are the mean diameter d, the channel height h and the channel length L, which are visualized in Figure 3.12.
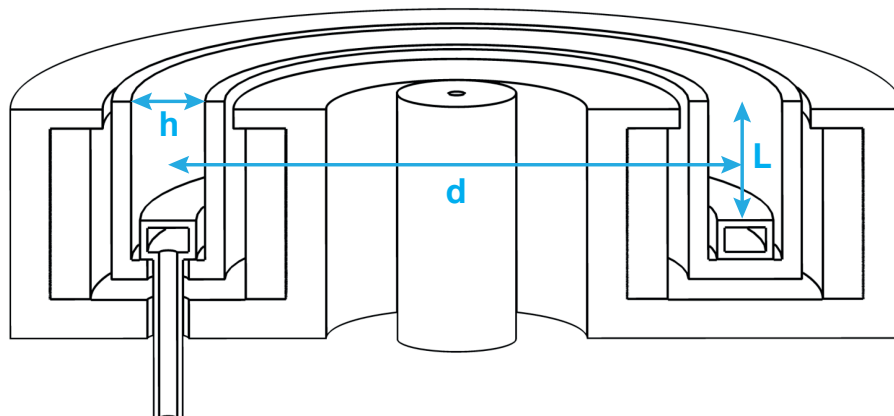
Figure 3.12: General definition of geometric parameters drawn in illustration from Raymond Liang [21]

3.3.1 Scaling Laws

One method of approaching a Hall Thruster design is the application of scaling laws. Theses scaling laws are identifying proportional relationships between the geometric parameters and operational values. They can be based on theoretically considerations as in [1] and by Dannenmayer [6] or purely empirically as in the work from Lee [19].

In both cases, the references are based on Xenon thrusters and while some relationships remain universal, especially determined coefficients can not be transferred to Oxygen wihtout changes.

Lee

In the work by Lee et al [19] in 2019, a set of Hall Thrusters was collected, ranging from 52 W to 1350 W. Over the geometric variables and operational values a fitting was performed on existing known theoretical relationships. The explicit scaling relationships solved for the geometric parameters are given in Equation 3.9 below. Notably no estimation is obtained for L, due to its independence to power, voltage or h and d but its involvement in the magnetic field B.

$$
\begin{aligned}
d &= \sqrt{\frac{P_d}{633.0 \cdot U_d}} \\
h &= 0.242 \cdot d \\
\dot{m}_a &= 0.003 \cdot hd \\
T &= 892.7 \cdot \dot{m}_a \cdot \sqrt{U_d}
\end{aligned}
\tag{3.9}
$$

By providing a desired power level as discharge power P_d and a discharge voltage U_d, the subsequent values can be determined.

Dannenmeyer

In the earlier work by Dannenmeyer [6] in 2011, no explicit numbers are supplied for the constants used in the published relationships, shown in Equation 3.10. However, this can be solved by simply plugging a reference thruster with known values into the equations to yield an estimation for the coefficients.

$$
\begin{aligned}
T &= C_{T1} \cdot \dot{m}_a \cdot \sqrt{U_d} \\
T &= C_{T2} \cdot \sqrt{U_d} \cdot d^2 \\
I_{sp} &= C_{I_{sp}} \cdot \sqrt{U_d} \\
I_d &= C_I \cdot d^2 \\
P &= C_p \cdot U_d \cdot d^2 \\
L &= C_L \cdot \lambda_i \\
h &= C_h \cdot d
\end{aligned}
\tag{3.10}
$$

This was done by the known values of the SPT-100, which yielded the constants. When now the equations are rearranged to describe the geometry, a thruster can be designed for a given power and voltage input.

Comparison

To give an impression of both scaling methods, the SPT series (SPT-100, SPT-70, SPT-50, SPT-30, SPT-25 and SPT-20) is plotted together in Figure 3.13 with both both scaling results. In this condition both scaling laws give almost identical results. In Table 3.2, an averaged solution between both scaling laws is given for multiple power points. It should be said however, that both scaling methods in its current form aren't calibrated for the high power domain, as the dataset for Lee ended at 1350 W and the coefficients of Dannenmayer have ben also determined by a 1350 W thruster. Therefore, the values for the high power GEO points should be taken as idea on size and thrust, rather than an accurate result.
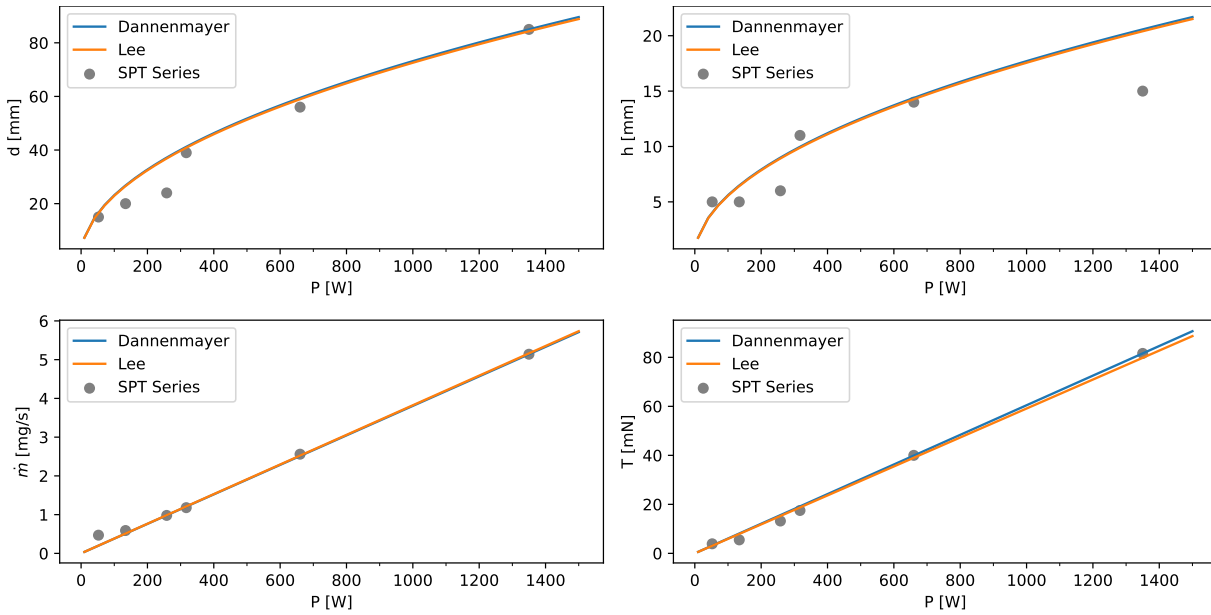
Figure 3.13: Power dependent scaling values of Lee and Dannenmayer with the SPT Series as Xenon reference

	var.	unit	demo		GEO	
input	P	kW	1	5	12	20
	U	V	300	300	300	300
output	d	mm	72.9	163	252	326
	h	mm	17.6	39	61	79
	$\dot{m}$	mg/s	3.8	19	46	76
	T	mN	59.8	299	717	1196

Table 3.2: Scaled geometry for a Xenon Thruster by averaged scaling law for the designed and GEO reference power points

3.3.2 Oxygen Reference

As by the time of writing only two Hall Thrusters have been designed and operated on Oxygen, which makes the sample for a comparison very small, especially as both of these are highly experimental and non-optimised. The first reference is from a japanese research group at Tokyo University already in 2003 by Nakagawa [24]. The second reference is from the Imperial Collage London on their water electrolysis thruster WET-HET by Schwertheim and Knoll [29] [28] and Tejeda [34].

In the following table the geometry of the two existing Oxygen thrusters are shown.

variable	unit	Tokyo	WET-HET
P	W	1000	180 - 2238
d	mm	55	25
h	mm	5	5
L_{test}	mm	[4, 7, 12, 14]	[5.5, 13.1, 34.8, 44.8, 59.8]
L_{opt}	mm	12	13.1

Table 3.3: Geometry of the two reference Oxygen thrusters from Tokyo [24] and London [34]

Notably, both of these thrusters don't fit the values of the Xenon scaling rules.

comparable states

In order to gain insight of these two reference thrusters, the first required step is to bring them in a comparable state on the targeted power level of 1000 W. As for the thruster from Tokyo some parts of information are assumed by context of the paper, as for example the power point was given as class, but not for the measurements. Fore the thruster from London, a wide range of data is available, which was used to interpolate the power point of interest. In Table 3.4 can be seen the comparable performance of both thrusters at a power point of 1000 W.

variable	unit	Tokyo	WET-HET
P	W	1000**	1000
U_d	V	350.	291.02*
$\dot{m}_a$	mg/s	1.16	0.958
I_{sp}	s	1000.	1497.83*
B	T	0.014	0.060
T	mN	11.375**	14.084*
η_T	%	9	10.37*

Table 3.4: Comparable performance of the two oxygen reference thrusters at 1kW (* linear interpolated, ** assumed by conntext)

There is some leftover incomparability by these two thrusters, as they are not sharing the same I_{sp}. Ion engines in general have a higher thrust efficiency under higher exit velocities due to the bigger portion of energy consumption during the acceleration phase, as mentioned in section 3.1 under "Sequence of Ionization". However, since they still share similar levels of I_{sp}, this state is seen as comparable.

3.3.3 Oxygen Design

As the WET-HET shows the higher efficiency and thrust, while having a higher I_{sp}, it is taken as point of reference and treated as improvement over the thruster from Tokyo. If the goal would be to simply reproduce the performance of the WET-HET, all geometric and electric properties could be copied. In order to explore more range of the spectrum and to attempt improving the thrust efficiency η_T further, two design changes are made by following previous trends.

Mean Diameter   The first trend is a negative correlation of the diameter and the thrust efficiency ($d \downarrow 55\% \Rightarrow \eta_T \uparrow 1.37\%$), when the two reference geometries (Table 3.3) are compared to the reference performance (Table 3.4). Whether this increase in efficiency is truly explained by the change of d, or if this trend also continues further down the line is unclear. However, a decrease in channel size as beneficial adaptation for Oxygen as propellant was already identified in the first investigation of the thruster from Tokyo [24], which is why this trend could be worth exploring.

As there was no change from the channel height of $h = 5\ mm$ from Tokyo to London, this conservation is kept, so that h remains on its reference value while the mean diameter is changed, which also explores a new surface to area ratio. This is also beneficial for manufacturability as even smaller structures can be avoided, as anode components that have to be placed inside the channel are getting to small.

Discharge Voltage   The second trend is a correlation of the discharge voltage U_d to the thrust efficiency η_T. On the first sight a comparison of the performance in Table 3.4 suggests a negative correlation, however if these dependencies are analyzed isolated for one thruster, a strong positive correlation to η_T present. However, in those cases the mass-flow was kept constant, so that this effect is overlapping with an increased efficiency on increased power. Therefore there is a remaining uncertainty.

Additionally, the discharge voltage U_d had a positive correlation to the propellant utilization η_p as well, which is highly desirable to be increased as the low propellant utilization was considered as main reason for the under-performance compared to Xenon (except dissociation losses) [24]. As an increase in voltage under a constant point of power would result in the reduction of mass-flow, the influence of the mass-flow needs to be taken into account as well. In Figure 3.14 are illustrated the two dependencies of voltage and massflow on the propellant utilization.
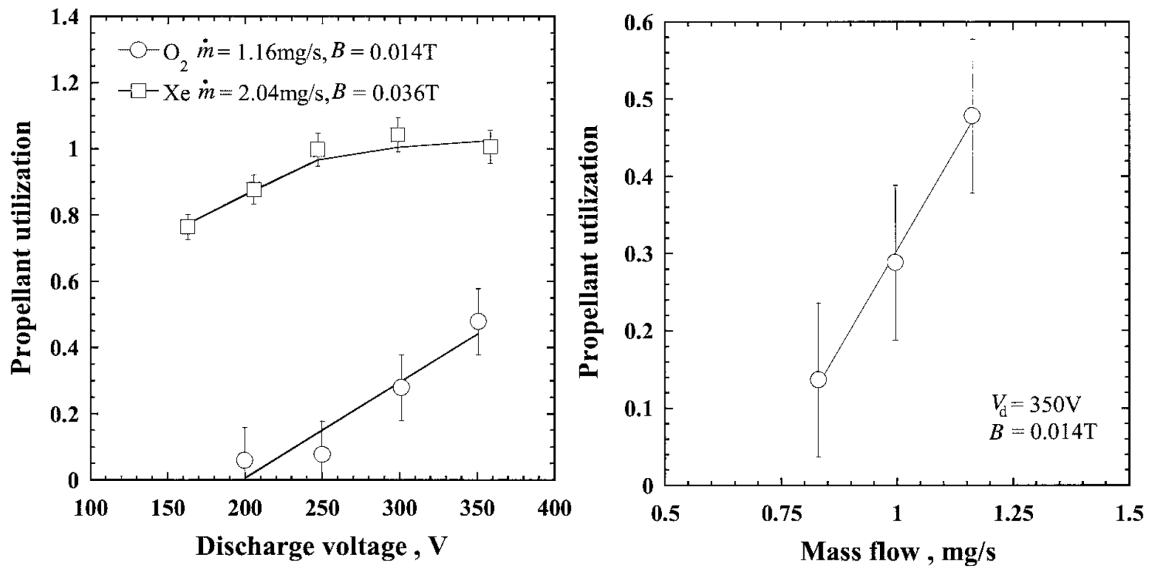
Figure 3.14: Dependencies of voltage and mass flow on propellant utilization - from original publication of Nakagawa [24]

As both feature a positive correlation, their rate of change needs to be compared to answer the question, whether an increase in voltage with a decrease in mass flow still expects an increase in the propellant utilization. In both cases, a power increase is overlapping the effect, which is assumed to roughly cancel out in this case. The rate of change is expressed in Equation 3.11.

$$\frac{\delta\eta_p}{\delta U_d} = 0.00289\ \frac{1}{V} \qquad\qquad \frac{\delta\eta_p}{\delta\dot{m}} = 1.03013\ \frac{1}{mg/s} \qquad\qquad (3.11)$$

These dependencies can be evaluated by the amount of volt and the amount of mass-flow to be changed. The determination of these amounts will be performed in the next section, but the resulting effect on η_p is shown here in advance in Equation 3.12. It shows that under a design increase of voltage, an increase of η_p is expected, despite the counteracting effect of the reduced mass-flow.

$$158.98\ V \cdot \frac{\delta\eta_p}{\delta U_d} = 0.45972 \qquad\qquad 0.188\ mg/s \cdot \frac{\delta\eta_p}{\delta\dot{m}} = 0.19367 \qquad\qquad (3.12)$$

Design

In order to compile both changes into a design and to estimate the resulting change of operational values, proportional relations are used. At this point an assumption is made, that scaling laws, as mentioned earlier for Xenon, are also existing for Oxygen but with different coefficients. These new scaling coefficients for Oxygen, C_{d*}, C_{m*} and C_{T*} are determined by the WET-HET reference over the relationships from Lee. This results in the experimental scaling set of Equation 3.13.

$$
\begin{aligned}
d &= \sqrt{\frac{P_d}{C_d \cdot U_d}} & C_{d*} &= 0.00548 \\
h &= C_h \cdot d & C_{h*} &= 0.2 \quad \text{to be altered} \\
\dot{m}_a &= C_m \cdot hd & C_{m*} &= 0.00766 \\
T &= C_T \cdot \dot{m}_a \cdot \sqrt{U_d} & C_{T*} &= 0.86182
\end{aligned}
\tag{3.13}
$$

This enables to compute changes on the design while expecting a similar efficiency from the scaling laws. To decide how far the voltage should be increased can not be easily justified, however if the positive trend of the correlation to the propellant utilization is followed, it would reach a value of $\eta_p = 1$ at 544 V. Realistically this trend will decay much earlier, but it should serve as point of reference. As the WET-HET was tested up to a voltage of around 350 V, the goal is here to reach into a new domain, which is why the design voltage is set to 450 V. This voltage might overshoot the optimal point, but should be seen as maximum voltage to be tested at. Also at 450 V the new diameter d, determined from the experimental Oxygen scaling laws is conveniently 20 mm. Together with the other equations from Equation 3.13 the new expected values are determined, with the exception of h and L.

This way the change of voltage $\Delta U_d = 158.98\ V$ and the change of mass-flow $\Delta \dot{m} = 0.188\ mg/s$ are computed, which have been required in the previous section to determine the expected effect on the propellant utilization.

As previously explained, h is kept constant against the scaling laws. And due to the fact that the magnetic field strength B is also preserved from the reference value, L is to be expected to be similar to the WET-HET. In fact, the optimal tested L_{opt} from Tokyo was 12 mm and for the WET-HET at 13.1 mm which is very close to each other, besides a great difference in B from 0.014 Tesla and 0.06 Tesla. This can be explained by the very big increment test size of the channel length for the WET-HET, where $L = 13.1$ mm was just better than 34.8 mm and 5.5 mm. To eliminate uncertainties like this, the thruster designed in this work will feature a step-less incrementation of the channel length L, so that a very accurate L_{opt} can be determined. To still constrain the channel length, a maximum of $L = 20$ mm was foreseen, which should contain the optimum somewhere around 13.1 mm from the WET-HET.

Geometry

The final design parameters are collected in Table 3.5 under comparison to the WET-HET.

variable	unit	WET-HET	Design Change	TUM	Δ
P	W	1000		1000	→
d	mm	25	↓ 5 mm	20	↓
h	mm	5		5	→
L_{test}	mm	[5.5, 13.1, 34.8, 44.8, 59.8]		[0 .. 20]	
L_{opt}	mm	13.1		?	
U	V	291.02*	↑ 159 V	450	↑
$\dot{m}$	mg/s	0.958		0.770**	↓
I_{sp}	s	1497.83*		1864.23**	↑
B	T	0.060		0.060	→
T	mN	14.084*		14.084**	↕
η_T	%	10.37*		10.37**	↕

Table 3.5: Comparison of the WET-HET and the designed thruster at TUM (* linear interpolated, ** estimated under experimental scaling law)

3.4 Plasma Simulation

3.4.1 Remarks on Plasma Physics

As a plasma is a state of freed or partially freed charges that interact with each other, an accurate description of plasma behaviour always comes down to an accurate description of each group of species. In a noble gas Hall Thruster mainly 3 of those species exists: neutrals, electrons and ions. But if for example wall interactions would be considered chemically, the relevant number of species would expand rapidly while new molecular bonds can be formed.

Due to the difference in mass between electron and ions, those two species can experience vastly different dynamics. One example is that under a high electromagnetic frequency electrons can be able to follow the perturbations which lead to the reflection of that wavelength, while the ions have just to much inertia to be influenced by it at all.

Further non obvious effects of plasma's are, that electric fields are naturally shielded and only interact in a short range defined by the Debye length. This can be explained by the charged particles which are re-arranging quickly, so that they oppose the external field. Many of these plasma phenomena have very small time constants, which sets requirements for a simulation. All together a full plasma simulation is a highly complex problem.

3.4.2 Software

One method to deal with the high number of entities in a plasma is the treatment as fluids, which divides the two main categories of plasma simulation software. Particle in Cell (PiC) as the approach to handle individual entities and magnetohydrodynamics as the approach of a continuous medium. Either way complex differential equations, often energy balancing equations need to be solved.

HETMAn

The software Hall Effect Thruster Modeling & Analysis (HETMAn) is a plasma simulation tool, designed specifically for Hall Thrusters. It was developed at Insitute of Plasma Physics and Laser Microfusion in

Warsaw, Poland by Serge Barral. The development of HETMAn code was partly funded by the European Commission (FP7 'HiPER' project, number 218859) and received support from the Foundation for Polish Science in the year 2011 as well as from Snecma in 2012. Under personal contact, i have been granted access to this code, which is normally not freely available. HETMAn is a 1D magnetohydrodynamic simulation which is described by a long set of governing equations shown in Figure 3.15 which are a mixture of Navier-Stokes and Maxwellian equation sets.

Neutrals

$$
\begin{aligned}
\frac{\partial n_{n1}}{\partial t} + \frac{\partial}{\partial x}\left(n_{n1}V_{n1}\right) &= -\beta_i n_e n_{n1} - \alpha_w \zeta n_{n1} V_{n1}, \\
\frac{\partial}{\partial t}\left(n_{n1}V_{n1}\right) + \frac{\partial}{\partial x}\left(n_{n1}V_{n1}^2 + n_{n1}\frac{T_c}{3m_n}\right) &= -\beta_i n_e n_{n1} V_{n1} - \alpha_w \zeta n_{n1} V_{n1}^2, \\
\frac{\partial n_{n2}}{\partial t} + \frac{\partial}{\partial x}\left(n_{n2}V_{n2}\right) &= -\beta_i n_e n_{n2} + \nu_{iw} n_e + \alpha_w \zeta n_{n1} V_{n1}, \\
\frac{\partial}{\partial t}\left(n_{n2}V_{n2}\right) + \frac{\partial}{\partial x}\left(n_{n2}V_{n2}^2 + n_{n2}\frac{T_c}{m_n}\right) &= -\beta_i n_e n_{n2} V_{n2} - \alpha_w \nu_{nw} n_{n2} V_{n2}.
\end{aligned}
$$

Ions

$$
\begin{aligned}
\frac{\partial n_i}{\partial t} + \frac{\partial}{\partial x}\left(n_i V_i\right) &= \beta_i n_n n_e - \nu_{iw} n_i, \\
\frac{\partial}{\partial t}\left(n_i V_i\right) + \frac{\partial}{\partial x}\left(n_i V_i^2\right) &= n_i \frac{e}{m_i} E + \beta_i n_i \left(n_{n1} V_{n1} + n_{n2} V_{n2}\right) - \nu_{iw} n_i V_i.
\end{aligned}
$$

Electrons

$$
\begin{aligned}
\frac{\partial n_e}{\partial t} + \frac{\partial}{\partial x}\left(n_e V_{ex}\right) &= \beta_i n_n n_e - \nu_{iw} n_i, \\
\frac{\partial}{\partial x}\left(n_e T_{e\perp}\right) &= -n_e e E - m_e n_e \left(V_{ex}\nu_e + V_{e\theta}\omega_{ce}\right), \\
\frac{\partial}{\partial t}\left(m_e n_e V_{e\theta}\right) + \frac{\partial}{\partial x}\left(m_e n_e V_{ex} V_{e\theta}\right) &= m_e n_e \left(V_{ex}\omega_{ce} - V_{e\theta}\nu_e\right), \\
\frac{\partial}{\partial t}\left(n_e \mathcal{E}_{e\parallel}\right) + \frac{\partial}{\partial x}\left(n_e V_{ex}\mathcal{E}_{e\parallel} - \kappa_\perp^\parallel \frac{\partial T_{e\parallel}}{\partial x}\right) &= Q_{e\parallel}, \\
\frac{\partial}{\partial t}\left(n_e \mathcal{E}_{e\perp}\right) + \frac{\partial}{\partial x}\left[n_e V_{ex}\left(\mathcal{E}_{e\perp} + T_{e\perp}\right) - \kappa_\perp^\perp \frac{\partial T_{e\perp}}{\partial x}\right] &= -e n_e V_{ex} E + Q_{e\perp}.
\end{aligned}
$$

Figure 3.15: HETMAn governing equations [15]

The software is used by providing a configuration file, where the thruster properties and all interaction parameters are supplied in an .xml file. This .xml file also contains an initial state, as this solver is an explicit propagation of the initial state. In detail, a hyperbolic system of conservation laws as hyperbolic partial differential equations are numerically solved in an explicit time integration. To ensure convergence of the derived solution, the Courant–Friedrichs–Lewy condition (CFL-condition) is deployed. This criterion essentially requires the time step resolution to be small enough to capture the changes on the spatial resolution. The criterion has the following form for a 1D case: $C = \frac{u\Delta t}{\Delta x} < C_{max}$, where C is a dimensionless number (Courant number), u the magnitude of the velocity, Δt the time step and Δx the length interval of the spatial grid. For explicit solvers C_{max} is typically set to 1.

In order to gain experience with this software, 9 test cases on the SPT-100 have been recreated. The test cases are on constant nominal voltage of $U_d = 300\,V$ with constant cathode mass flow of $0.26\,mg/s$ and variable anode mass flow in 9 points from $3.45\,mg/s$ to $5.64\,mg/s$. For the initial configuration file, the provided SPT100.xml example file was utilized and the mass flow rate was set to the value of the test case from NASA. All simulations are run on three different time steps dt to ensure that the long term solution converges where their output behaviour is shown in Figure 3.16 and Figure 3.17. For the test cases 1 to 3 it can be seen that the discharge current I_d in the end (on the right) converges as a damped oscillation into a static value.

Figure 3.16: HETMAn simulation results, discharge current over time for different NASA test cases 1 to 5 on the SPT-100

In the test cases 4, a new mode can be observed, as remaining oscillations at roughly 200 kHz are present. These oscillations increase in amplitude when the mass flow is increased further in case 5 and 6. This high frequency mode of oscillation is known under ion transit oscillations, which can range from 100 kHz to 500 kHz.

When proceeding to case 7 again a new oscillation mode can be observed. This time a lower frequency oscillation at roughly 16 kHz is super imposed with the previous Ion transit oscillations. These lower frequency oscillations are known under the breathing mode which can range from 5 kHz to 30 kHz. Again the amplitude of the new mode is increasing in amplitude when the mass flow is further increased to case 8 and 9. As the power oscillations have been risen over ± 30 W (case 4), ± 68 W (case 5), ± 98 W (case 6) for the ion transit oscillations, the power oscillations for the breathing mode are substantially higher with ± 255 W (case 7), ± 525 W (case 8) and ± 660 W (case 9).

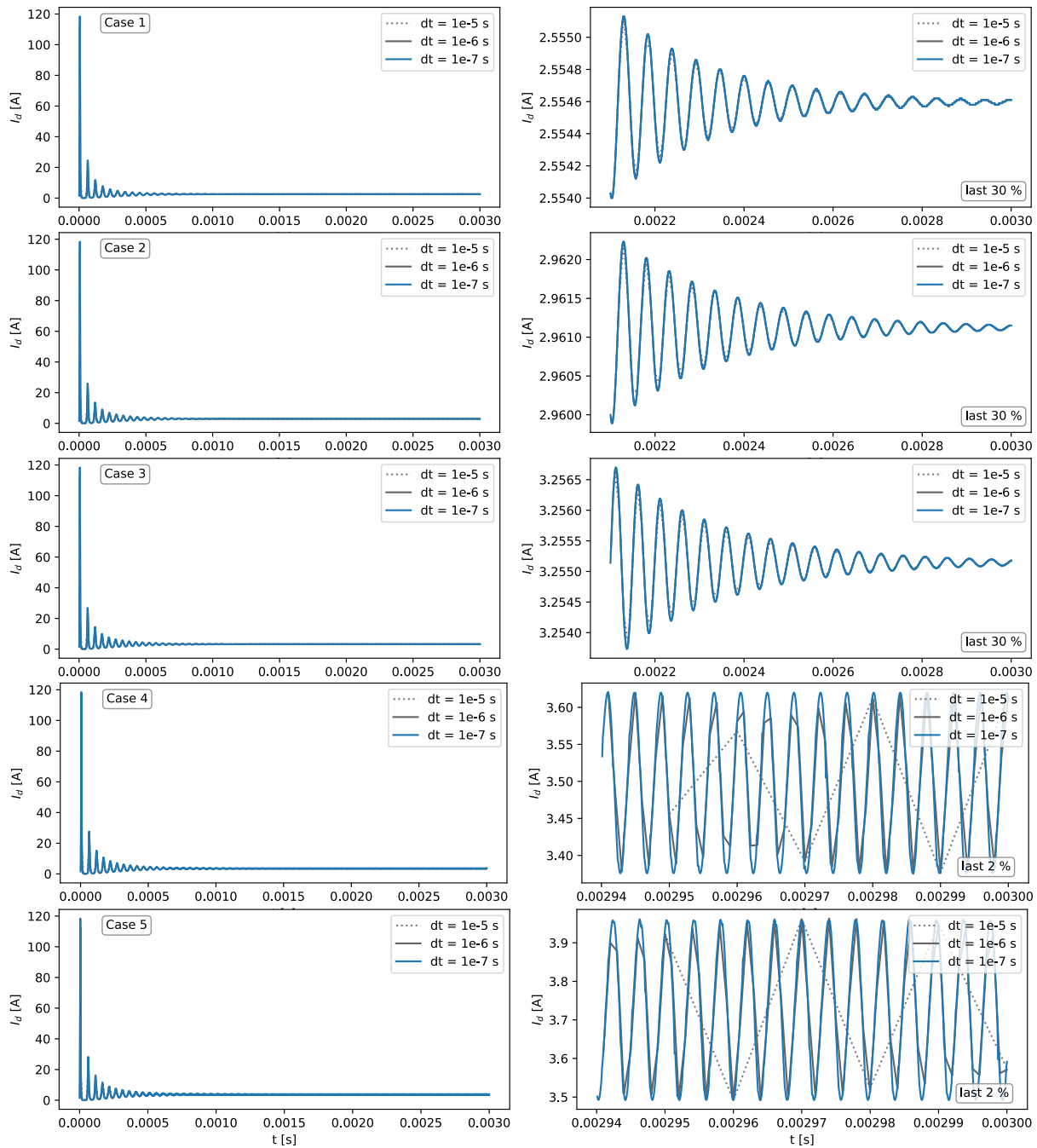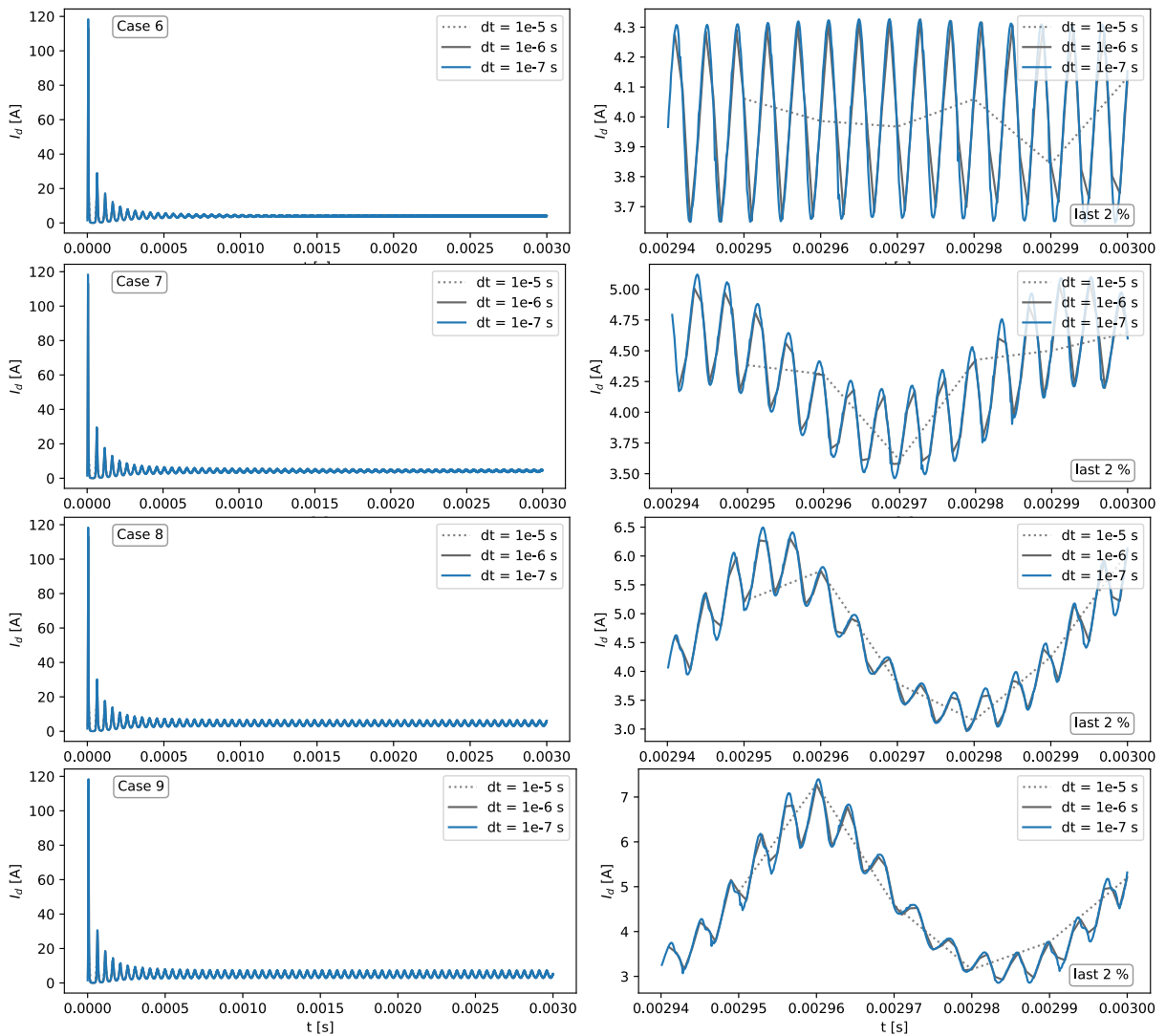**Figure 3.17:** HETMAn simulation results, discharge current over time for different NASA test cases 6 to 9 on the SPT-100

When the simulation results are compared to the NASA measurements in Table 3.6, the results are mixed, as for example the thrust is predicted very accurately with $\leq 3\%$ deviation, if case 1 is neglected.

On the other side I_{sp} and η are estimated very poorly with 12% to 49 % deviation, if case 1 is neglected. Power is estimated rather well with 5% to 9 % deviation, if case 1 is neglected.

	Method	Voltage $U[V]$	Anode Massflow $\dot{m}_a[mg/s]$	Cathode Massflow $\dot{m}_c[mg/s]$	Power $P[W]$	Thrust $T[mN]$	Specific Impulse $i_{sp}[s]$	Efficiency η
		Input			Output			
1	NASA	300.		0.26	903.0	44.3	1220.0	0.293
	HETMAn	300	3.45	-	766.4	51.6	1736.0	0.652
					Δ -15%	Δ +16%	Δ +42%	Δ +123%
2	NASA	300.		0.26	975.0	58.8	1450.0	0.430
	HETMAn	300	3.87	-	888.3	60.0	1751.6	0.642
					Δ -9%	Δ +2%	Δ +21%	Δ +49%
3	NASA	300.		0.26	1050.0	64.1	1480.0	0.441
	HETMAn	300	4.17	-	976.5	66.0	1762.4	0.638
					Δ -7%	Δ +3%	Δ +19%	Δ +45%
4	NASA	299.		0.26	1120.0	68.6	1490.0	0.453
	HETMAn	300	4.42	-	1049.7	70.9	1768.2	0.633
					Δ -6%	Δ +3%	Δ +19%	Δ +40%
5	NASA	299.		0.27	1190.0	72.8	1510.0	0.464
	HETMAn	300	4.66	-	1118.7	75.2	1768.4	0.626
					Δ -6%	Δ +3%	Δ +17%	Δ +35%
6	NASA	299.		0.26	1270.0	78.2	1540.0	0.467
	HETMAn	300	4.93	-	1196.7	80.0	1769.3	0.620
					Δ -6%	Δ +2%	Δ +15%	Δ +33%
7	NASA	299.		0.26	1350.0	82.7	1550.0	0.464
	HETMAn	300	5.18	-	1270.0	84.5	1768.9	0.614
					Δ -6%	Δ +2%	Δ +14%	Δ +32%
8	NASA	299.		0.26	1420.0	86.6	1550.0	0.478
	HETMAn	300	5.42	-	1342.5	88.8	1767.7	0.607
					Δ -5%	Δ +3%	Δ +14%	Δ +27%
9	NASA	299.		0.26	1490.0	91.7	1580.0	0.452
	HETMAn	300	5.64	-	1395.3	91.9	1767.0	0.607
					Δ -6%	Δ +0.2%	Δ +12%	Δ +34%

Table 3.6: HETMAn simulations versus test case measurements on the SPT-100 from NASA [5]

HallThruster.jl

A great alternative to mostly proprietary Hall Thruster simulation software is the open source package written in Julia "*HallThruster.jl*". This software got very recently published in 2023 by researchers at the University of Michigan from the Plasmadynamics & Electric Propulsion Laboratory (PEPL) [22]. Their segment of electric propulsion and facility are one of the biggest in the world and feature state of the art developments such as nested thrusters, as the X3 which operated up to a power level of 100 kW in a research project with NASA [12].

Just as HETMAn, this package only supports inert gases for simulation, such that an analysis on Oxygen can not be easily done. Considering Oxygen being a highly exotic usage of Hall Thruster propellant, there is no explicit Hall Thruster simulation software for Oxygen available to the date of writing. However, through adaptations of simulators as HETMAn or HallThruster.jl, this could be perhaps reached more efficiently than a development from scratch. The open source code base makes HallThruster.jl the leading choice for such an endeavour.

3.4.3 Oxygen Adaptations

As it initially was planned to iterate the Oxygen thruster design through plasma simulations, it turned out that even simulations on conventional Xenon thrusters have a rather high amount of inaccuracy. It was identified that a reasonable simulation for Oxygen can only be done by considering the additional plasma reactions in the simulation. The plasma reactions that would need to be introduced are listed in Table 3.7 and pose a major piece of work to implement, as it requires not only to adapt ionization energies but the handling of completely new entities with new interactions to other species. This requires modification in the source code at the level of the governing equations, which would be a task that fills a PhD. If attempted, every reaction of Table 3.7 has a probability defined by the cross section, which is dependent on the energy demand of the reaction together with the energy distribution of the involved entities. In the end the initially planned sections in the task description turned out to be unattainable, which is why the thruster was then designed without iterations on plasma simulations.

base entity	Description	plasma collision reaction		
O_2	Dissociation	$O_2 + e^-$	$\rightarrow$	$O + O + e^-$
	Excitation	$O_2 + e^-$	$\rightarrow$	$O_2^* + e^-$
	Ionization	$O_2 + e^-$	$\rightarrow$	$O_2^+ + 2e^-$
	Attachment	$O_2 + e^-$	$\rightarrow$	O_2^-
	Dissociative Ion.	$O_2 + e^-$	$\rightarrow$	$O^+ + O + 2e^-$
	Dissociative Att.	$O_2 + e^-$	$\rightarrow$	$O^- + O$
O	Recombination	$O + O$	$\rightarrow$	O_2
		$O + O + O$	$\rightarrow$	O_3
	Ionization	$O + e^-$	$\rightarrow$	$O^+ + 2e^-$
		$O^+ + e^-$	$\rightarrow$	$O^{2+} + 2e^-$
		$O^{n+} + e^-$	$\rightarrow$	$O^{(n+1)+} + 2e^-$
	Attachment	$O + e^-$	$\rightarrow$	O^-
		$O^- + e^-$	$\rightarrow$	O^{2-}
		$O^{n-} + e^-$	$\rightarrow$	$O^{(n+1)-}$
	Excitation	$O + e^-$	$\rightarrow$	$O^* + e^-$
O_3	Dissociation	$O_3 + e^-$	$\rightarrow$	$O + O_2 + e^-$
	Excitation	$O_3 + e^-$	$\rightarrow$	$O_3^* + e^-$
	Ionization	$O_3 + e^-$	$\rightarrow$	$O_3^+ + 2e^-$
	Attachment	$O_3 + e^-$	$\rightarrow$	O_3^-

Table 3.7: Oxygen base entities and their plasma reactions with electrons and other neutrals

3.5 Materials

In this chapter the selected materials to construct the Hall Thruster parts from are specified and their functionality is discussed.

3.5.1 Discharge Channel

The material of the discharge channel is of great importance as it is in constant exchange to the plasma, which influences its properties and the thrusters efficiency subsequently. In previous works Boron Nitride (BN) was identified to be a superior choice to for example Aluminium oxide (Al_2O_3) [29]. Boron Nitride exists in several compositions and crystaline structures, which are denoted short as Grades.

As channel material for an Oxygen Hall Thruster BN Grade AX05 and BNSiO2 Grade M26 are the currently best known candidates. The properties of both are compared in Table 3.8.

Grade AX05 consists basically purely out of Boron Nitride, while Grade M26 has a 40 % Silicon dioxide composition. This part of Silicate results in a hydrophobic property of the BNSiO2 Grade M26, which is a great deal in the context of WEP, as the gases from the Electrolyzer contain humidity.

This is the reason why BNSiO2 Grade M26 ceramic is selected to manufacture the discharge channel. This material can be bought commercially at suppliers as Saint-Gobain [3], which also provide additional tips for machining this ceramic [4].

property	unit	BN Grade AX05	BNSiO2 Grade M26
composition		>99.5% hexagonal BN	60% BN, 40% SiO2
max. use temperature	$°C$	850	1000
thermal conductivity	$W/(m \cdot K)$	130	14
density	g/cm^3	1.9	2.1
hydrophobic		no	yes

Table 3.8: Material Properties of two types of Boron Nitride as wall material (Grade M26 selected)

The designed discharge channel is displayed in Figure 3.18 which will be secured by 4 screws from the top of the thruster.
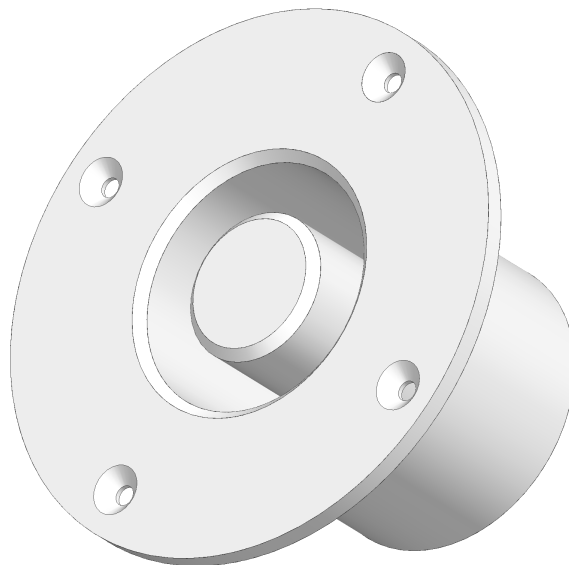

Figure 3.18: Discharge channel out of Boron Nitrate Grade M26 (BNSiO2)

3.5.2 Magnetic Body

The magnetic body is designed to handle the main magnetic flow, while also providing structural integrity. It is an assembly of components which are shown and defined in Figure 3.19.
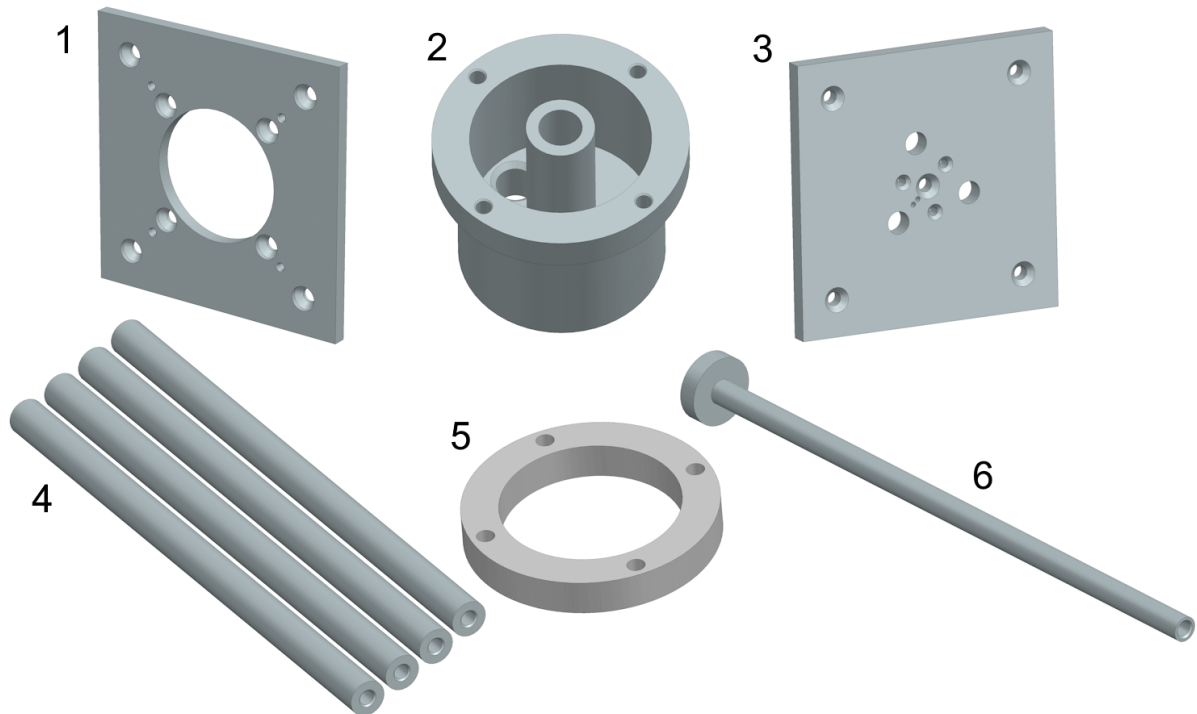

Figure 3.19: Components of the magnetic body, not to scale: 1) top plate, 2) center piece, 3) bottom plate, 4) 4x outer pole, 5) spacer, 6) inner pole

In this assembly, the spacer is aimed to be not magnetic while the inner pole is aimed to be especially magnetic, while the rest should conduct magnetic field decently. The bottom plate can hereby serve as structural mounting point, in which additional holes can be screwed without compromising the magnetic functionality.

Steel in general is a versatile option, as it can be either austenitic and show practically no magnetic behaviours, as also martensitic or ferritic with different magnetic properties present. Through design iterations in the Magnetic design 3.6, the inner pole was required to be made out of Supermalloy, a special alloy which is used in solenoid cores due to its exceptional magnetic properties.

For the spacer, non magnetic 316 Steel (1.4401) was chosen while the rest of the components have been assigned to the magnetic 1006 Steel (1.0313). In this assembly, which is held together by screws, it is important to mention that some of the screws are designed to be magnetic while others are designed to be not magnetic. To leave the option open for the procurement, the screw material is only required to fulfil their requirement on magnetism. If however a specification of material is required, then the magnetic screws are to be made from 1006 Steel (1.0313) while the non-magnetic screws from 316 Steel (1.4401).

A comparison of the three selected materials and their magnetic properties is shown in Table 3.9. A full assembly of the magnetic body with a cross-sectional view is shown in Figure 3.20.

property	unit	Supermalloy	1006 Steel (1.0313)	316 Steel (1.4401)
chemical composition	% Element	75 Ni 20 Fe 5 Mo	0.7 C 0.4 Mn 0.3 Si 0.3 Cu 0.2 Cr 0.25 Ni ...	0.07 C 2 Mn 1 Si ... 17.5 Cr 11.5 Ni 2.5 Mo ...
density	g/cm^3	8.7	7.85	7.9
magnetic conductivity		extremely high	high	low
B-H curve		non-linear	non-linear	linear
relative permeability	$\mu_r = \mu/\mu_0$	$\approx 500{,}000$	1404	1

Table 3.9: Material Properties of Supermalloy, 1006 Steel (1.0313) and 316 Steel (1.4401) as magnetic assembly material
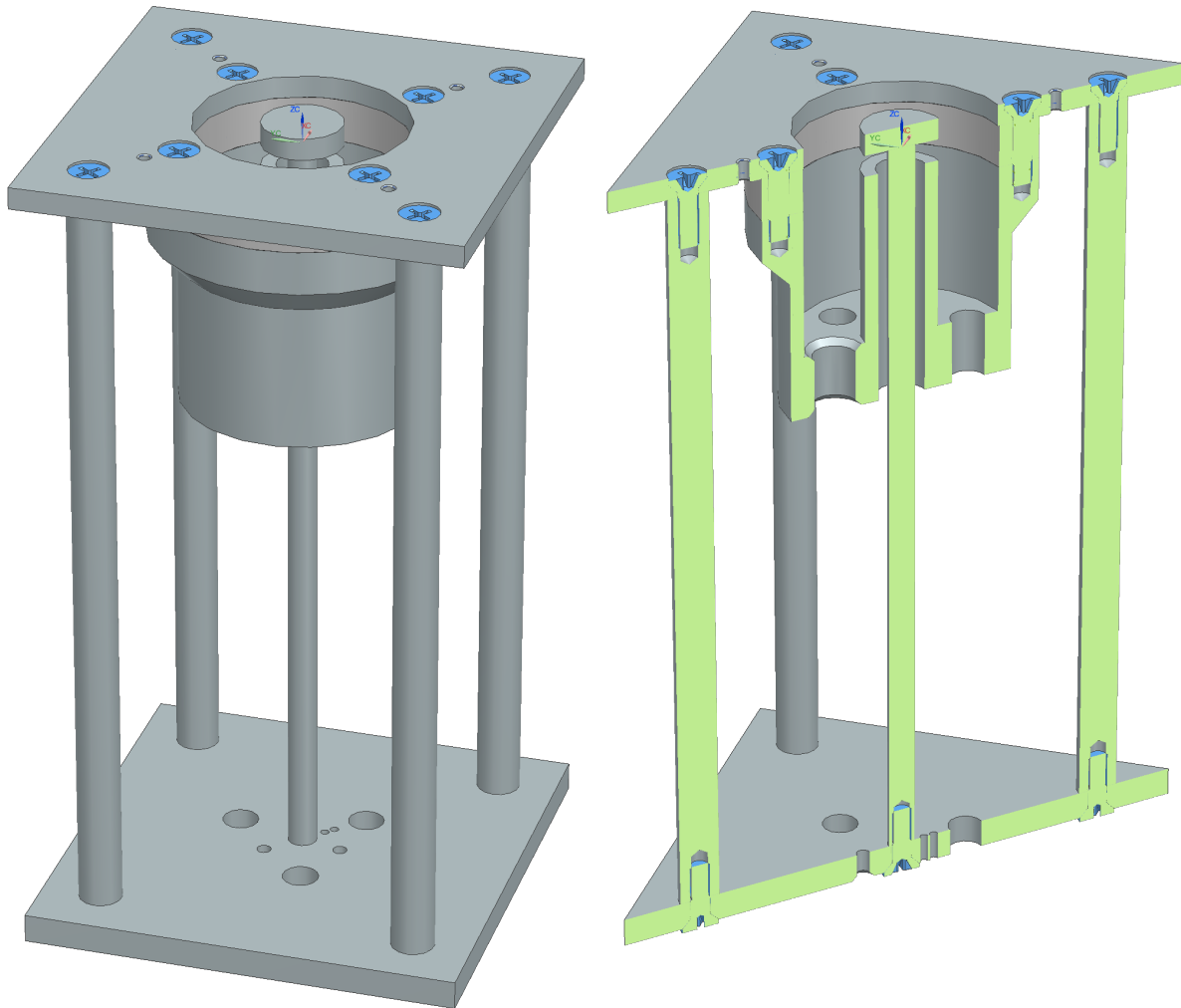

Figure 3.20: Assembled magnetic body from all body components with non-magnetic and magnetic screws
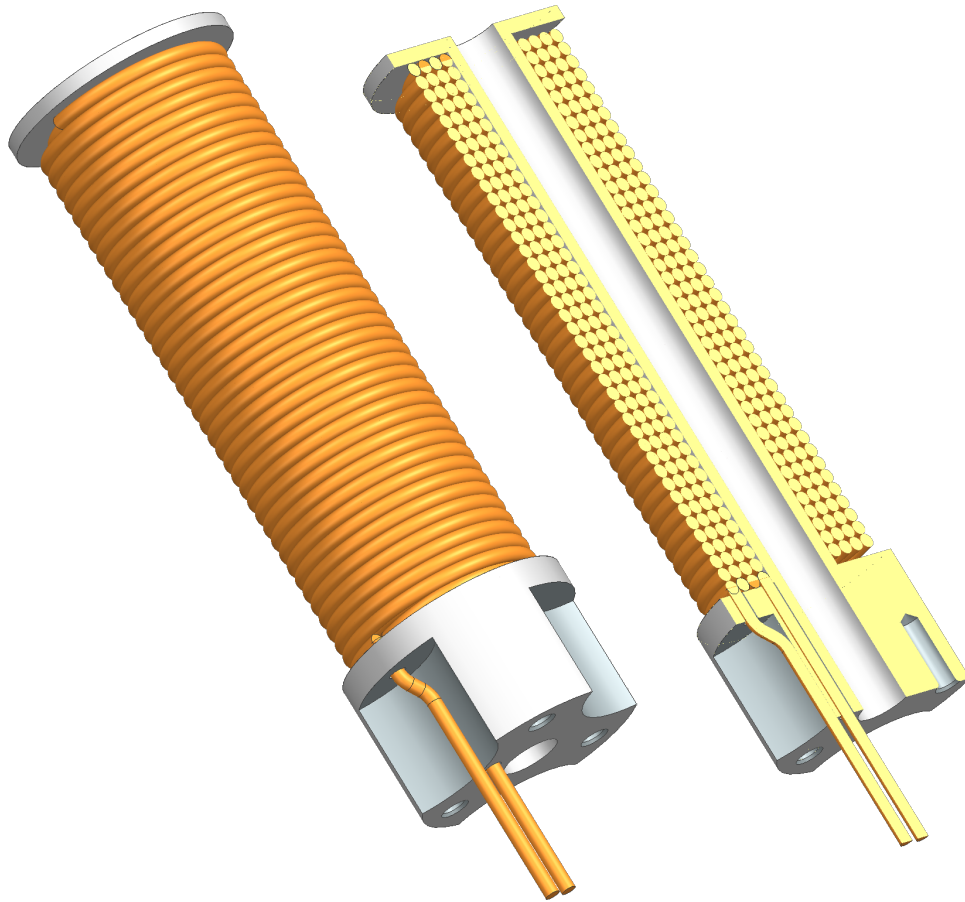
3.5.3 Magnetic Coil

Figure 3.21: Coil with 4 layers of 1 mm Copper wire in 41 mm winding space, resulting in 160 turns on its Aluminium coil case with cable feed through and mounting holes to the bottom plate

The Copper coil in Figure 3.21 is driven only by direct current (DC) and not by alternating current (AC), therefore the resistance of the coil is simply the ohmic resistance of the length of the coil wire. By its wire length of $l = 5.068\ m$ and its diameter of 1 mm, and therefore area A, the resistance R (Equation 3.14) is given depending on the materials resistivity ρ:

$$R = \rho \cdot \frac{l}{A} \tag{3.14}$$

This resistivity ρ is temperature dependent (Equation 3.15) and is determined by a reference resistivity ρ_0 at a reference temperature T_0 and a temperature coefficient α. For copper these values are for $T_0 = 20°C$, $\rho_0(T_0) = 0,0244\ \Omega \cdot mm^2/m$ and $\alpha = 0.0039\ K^{-1}$.

$$\rho(T) = \rho_0(T_0) \cdot (1 + \alpha \cdot (T - T_0))) \tag{3.15}$$

As in chapter 3.6 determined, a constant current of $I = 5.5\ A$ is required to achieve the desired magnetic field strength. Together with the temperature dependent resistance of the coil, the expected voltage and power demand are computed and illustrated in Figure 3.22.
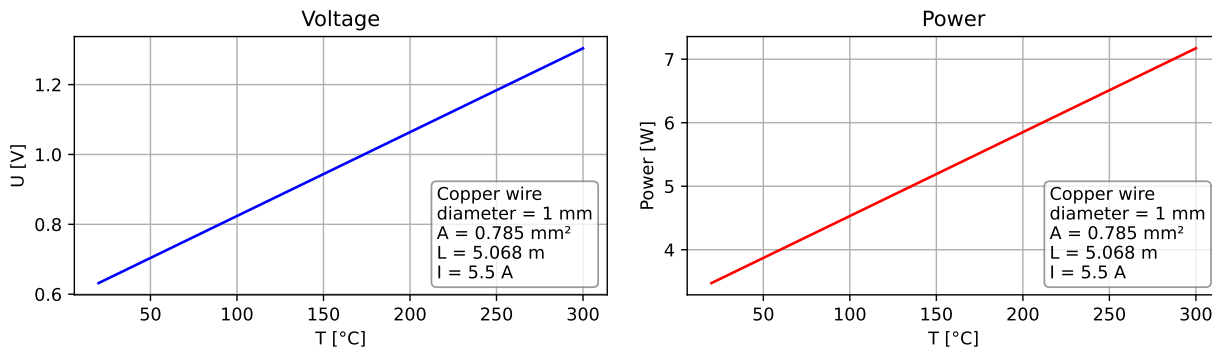
Figure 3.22: Coil operating voltage and power consumption depending on temperature

Whether the selected wire diameter of 1 mm is truly sufficient to maintain 5.5 A during operation can only finally be answered by the knowledge of the operating temperature if it surpasses the heat restrictions of the enamelled cover material or not. The heat classification for enamelled copper wires with Polyesterimid is 200°C when followed IEC 60317-13, which has a softening temperature of $\geq$340°C. This means the coil can be operated at 200°C for an extended amount of time and are aimed to be not much higher than that. To counteract high temperatures, the coil mount is made from Aluminium to give a good heat conduction to the bottom plate, which is serving as radiator. In general uses the current-carrying capacity of a 1 mm enamelled copper wire is given with 12 A in DIN VDE 0298 for multi line wires, however since 40 lines and 4 layers are making up the coil, the aluminium cooling element is most probably required to achieve a tolerable temperature.

As a reverse effect, the voltage needed to drive the coil in constant current mode can be translated directly to the temperature of the coil and therefore can serve as a temperature sensor. Due to additional wiring to the lab power supply could distort this measurement, this additional resistance should be significantly lower than the coil which is between 0.115 Ω (20°C) and 0.193 Ω (200°C).

3.5.4 Gas Connector

To connect the thruster to a feed line, a 1/16" NPT thread is foreseen at the center piece, where the connector can be screwed in. Due to lack of space in the underside of the thruster, an elbow connector piece was selected that guides a 90° turn. This connector is the SS-LM-FL1-NS1 tube fitting [7], which connects to a 1/16" pipe system.

3.5.5 Anode

The anodes main requirements come down to its electrical conductivity, its face plane interaction with the plasma and the chemical exposure to Oxygen. As high energy electrons are streaming on the face plane of the anode, this material is experiencing high erosional stress as this is essentially identical to destructive manufacturing methods for microanalysis or electron beam lithography where high speed electrons erode the surface. Besides slowly dissolving the anode, the loosened elements by erosion are negatively influencing the plasma, which is why a material of high resistance to erosion is beneficial for this application. Due to the kinetic energy of the electrons or Oxygen anions is also dissipated as heat on the face plane, additionally to radiative heat from the hot plasma itself, very high temperatures at

the face plane are the result. The current best fit of material, which is highly resistant to temperature and erosion is Tungsten, which is also used in other Hall Thrusters, as in the one from London.

Tungsten is furthermore extremely dense and hard which makes it a tough material to work with, which can be seen in the material properties table 3.10. Together with its mediocre electrical conductivity, Copper is chosen as the larger anode body and Tungsten as used face plate material as illustrated in Figure 3.31. Copper holds excellent electrical conductivity, a reasonable melting point and its emerging oxide layer is protecting further oxidation.
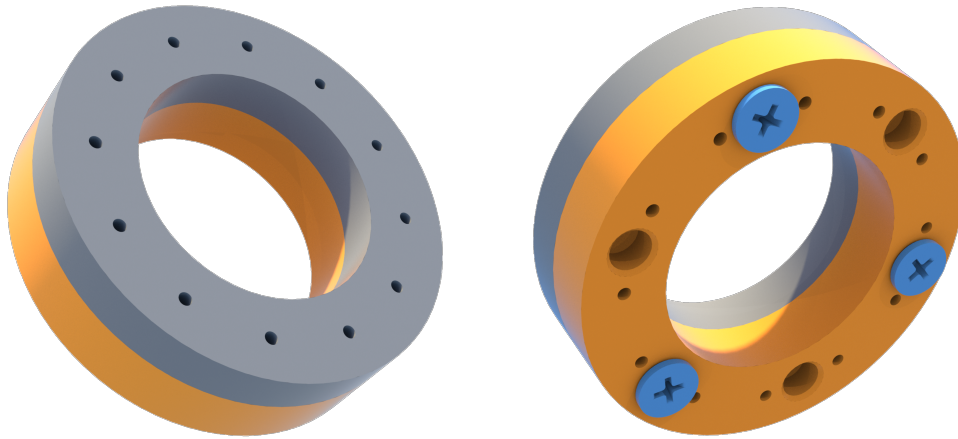

Figure 3.23: Anode with a Tungsten face plate (left) and Copper body with mounting holes for Copper threaded rods (right)

property	unit	Copper	Tungsten
melting point	°C	1085	3422
electrical conductivity	S/m	$58.1 \cdot 10^6$	$18.52 \cdot 10^6$
thermal conductivity	$W/(m \cdot K)$	400	170
hardness		3	7.5
density	g/cm^3	8.96	19.25
magnetism		dia-magn.	para-magn.

Table 3.10: Material Properties of Copper and Tungsten as anode material

The Oxygen gas is designed to gather under the anode as a small buffer chamber and then to flow out into the discharge channel through the drilled holes. The two metal discs are joined together by three DIN 7500 M2x5 screws from the underside, while three 3 mm threaded copper rods are inserted into the threaded holes of the copper body. The three threaded copper rods are the key to the step-less adjustment of the discharge channel length, as the whole anode can be displaced, when the nuts are loosened.

In order to achieve a seal on these copper threads, Polytetrafluoroethylene (PTFE) washers [35] and PTFE sealing nuts [30] are used to press against the threads and the center piece. This point of connection together with the sealing nuts is shown in Figure 3.24

PTFE was chosen as the washers need to fulfil electrical insulation from the anode to the rest of the thrusters body, as well as high temperature resistance and sealing abilities.
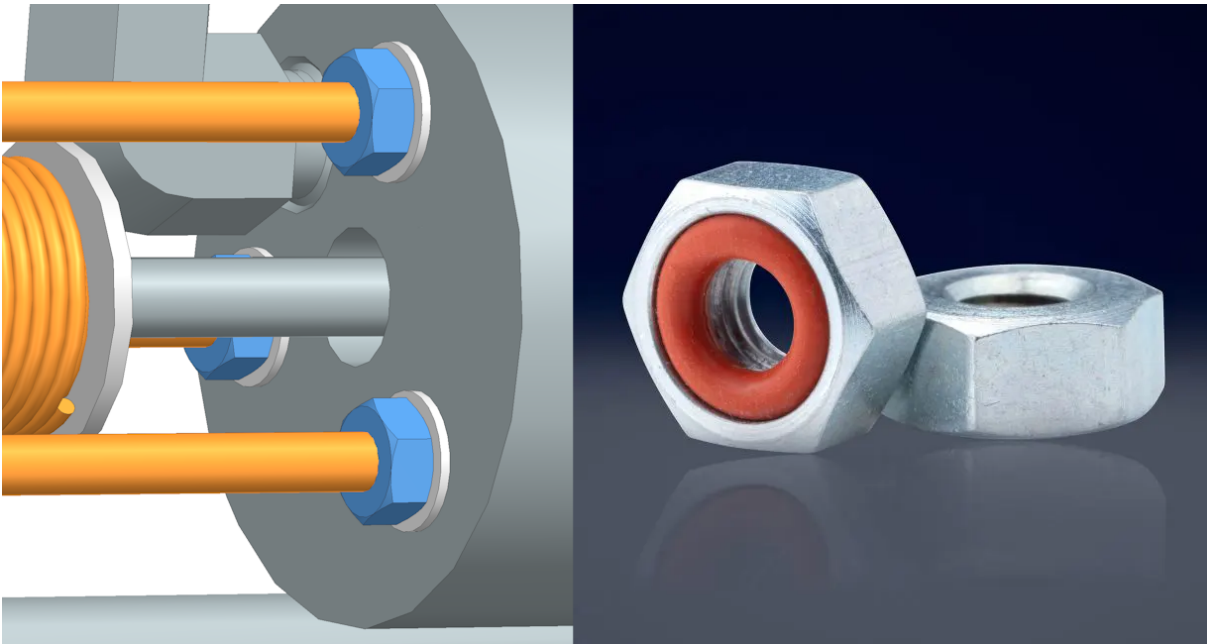
Figure 3.24: Sealed connection of anode copper threaded rods to center piece with PTFE washers and PTFE sealing nuts (Product photo from ZAGO [30])

The mechanism for the step-less adjustment can be seen best in the cut section view in Figure 3.25, where the position of the anode is stiffly connected to the copper rods which are able to slide horizontally when loosened by the nuts and washers.

Figure 3.25: Cut section view of the assembled Hall Thruster with step-less adjustment of channel depth

3.6 Magnetic Design

As described in chapter 3.1, the magnetic field is the core component for confinement and the ExB drift. The location of interest is the magnetic field intensity at the center of the discharge channel from the exit plane to the anode, which determines the plasma behaviour in the discharge channel. The r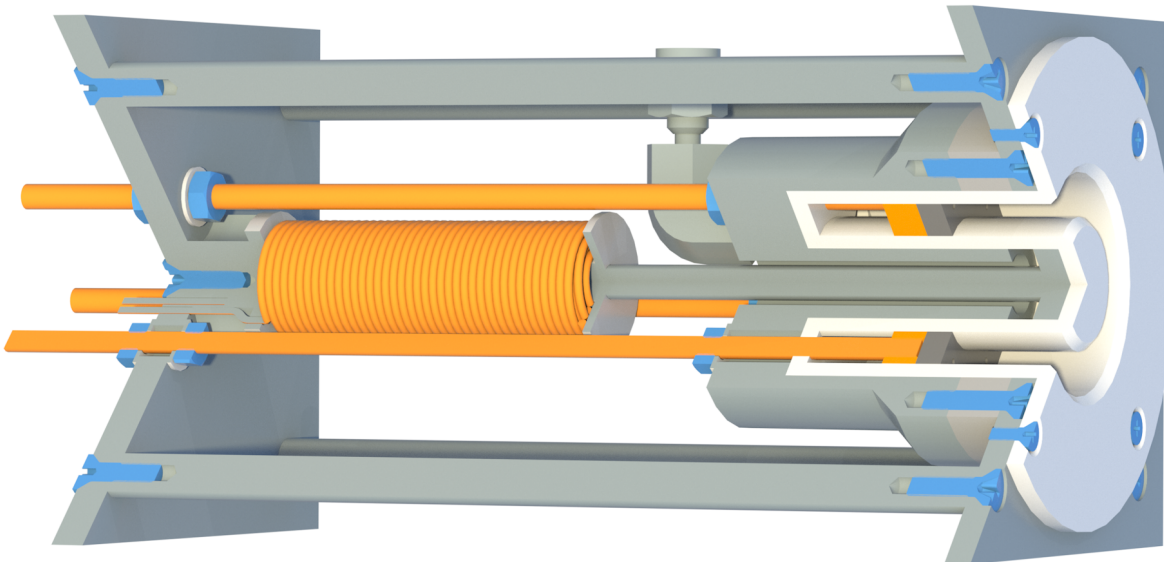equirements on the magnetic field characteristics are two fold. First, the desired radial magnetic field has to reach the aimed design value, which is 0.06 Telsa in this case. Second, a certain amount of magnetic shielding is aimed to be achieved, which proved to be very beneficial to performance on all Hall Thrusters. This magnetic shielding is describing the fast decay of magnetic field intensity when approaching the anode, which is reached by giving the magnetic field an alternative way to pass to the other side. The origin of the magnetic field will be an electromagnetic coil, which holds itself open variables of diameter, number of turns, coil current or which solenoid core material is getting used. The achievement of the combined requirements can be determined and iterated best through a magnetic simulation.

FEMM

The freely available Finite Element Method Magnetics (FEMM) software [10] was used to iterate the design of the magnetic materials and geometric configurations. This software is very efficient in achieving just that, however it is a 2D simulation which assumes radial symmetry in the case of the Hall Thruster. This requirement of the simulation on radial symmetry was the reason to place the coil on the center pole. If it would be placed on the outer poles, it wouldn't be radial symmetric anymore and the simulation would need to be carried out in a true 3D magnetic simulation as in COMSOL Multiphysics for example. The placement of four coils on the outer poles, instead one coil on the inner pole, would bring several benefits, but is rejected for the benefit of computability. One benefit of a single central coil is the simplicity of the control over the magnetic field.

During the design iteration it proved necessary to use not only magnetic steel for the center pole but a material with a much higher magnetic permeability (Supermalloy) in order to achieve the desired field strength on the maximum point in the discharge channel. As visible in Figure 3.26, the core material needs to conduct the magnetic field to the top of the thruster as efficient as possible, as otherwise it remains a strong choke point for the system.

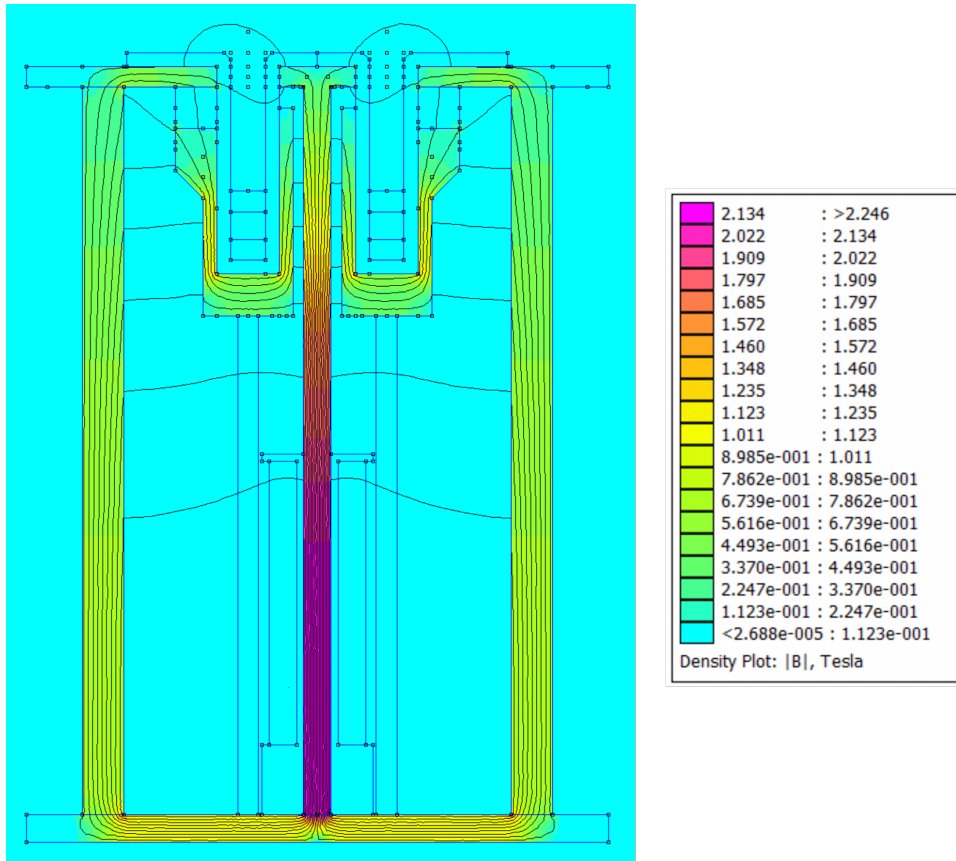**Figure 3.26:** Core magnetic flux in FEMM simulation of the magnetic body at 5.5 Ampere

In Figure 3.27 can be seen the great difference in magnetic properties of the magnetic steel and the Supermalloy, which both have a non linear B-H curve, but the Supermalloy results in magnitudes greater permeability.
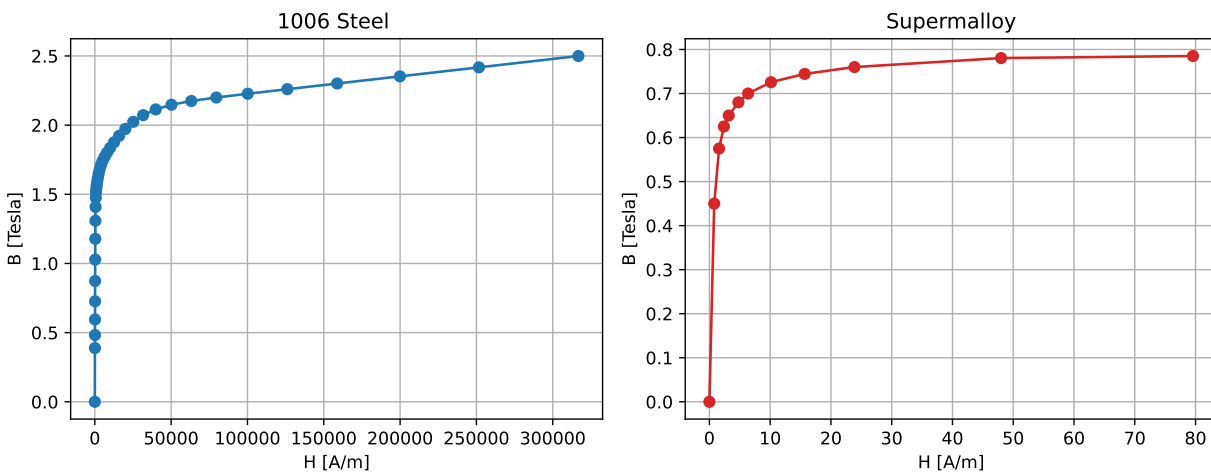
Figure 3.27: B-H curve of 1006 Steel (left) and Supermalloy (right), data from FEMM material library

The main result of the magnetic field design is shown in Figure 3.28, where a high magnetic field intensity is given near the exit plane, while featuring a fast decay towards the anode.
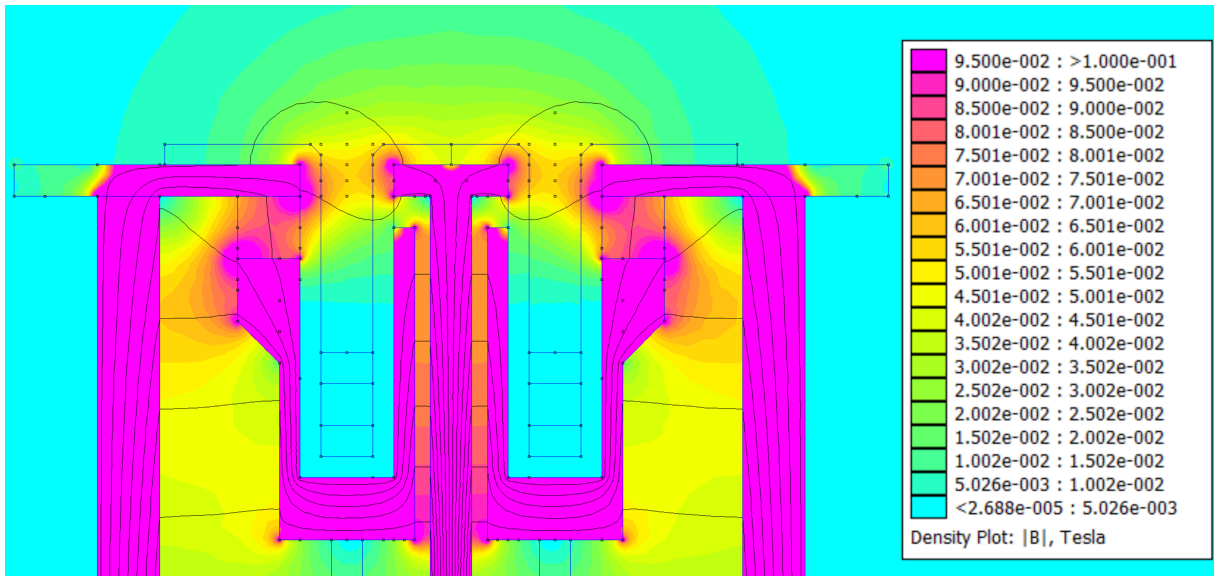
Figure 3.28: Channel magnetic flux in FEMM simulation of the magnetic body at 5.5 Ampere

The final magnetic geometry was simulated for multiple levels of coil current. The different achievable field strengths and characteristics can be seen in Figure 3.29.
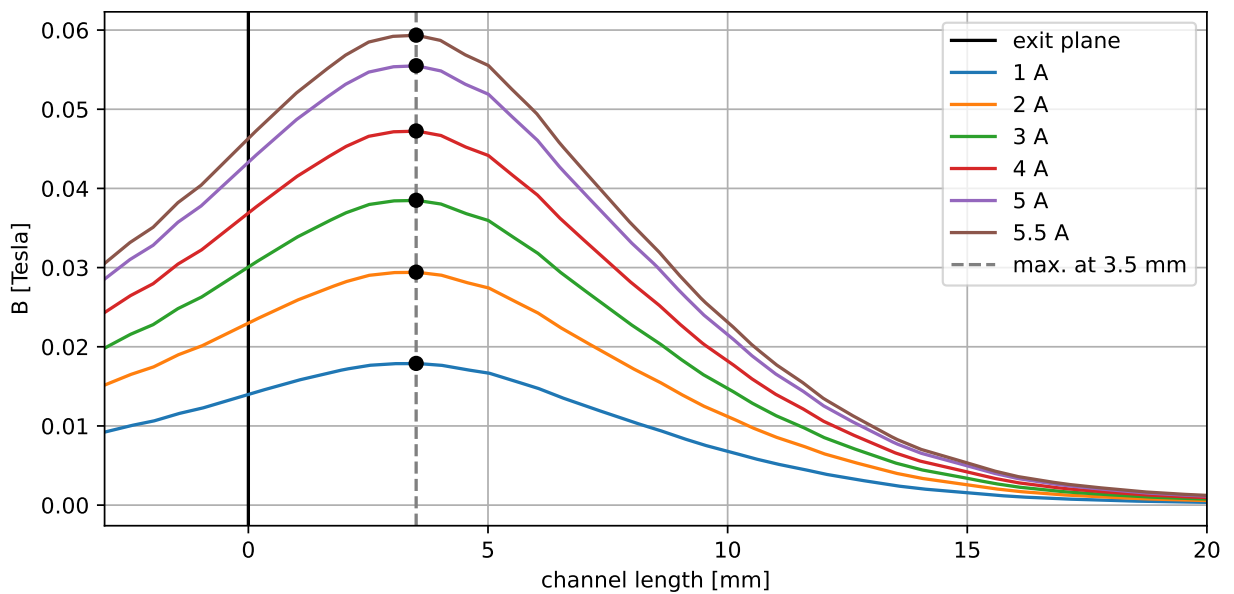
Figure 3.29: Magnetic flux over the center of the discharge channel for several coil currents

3.7 Results
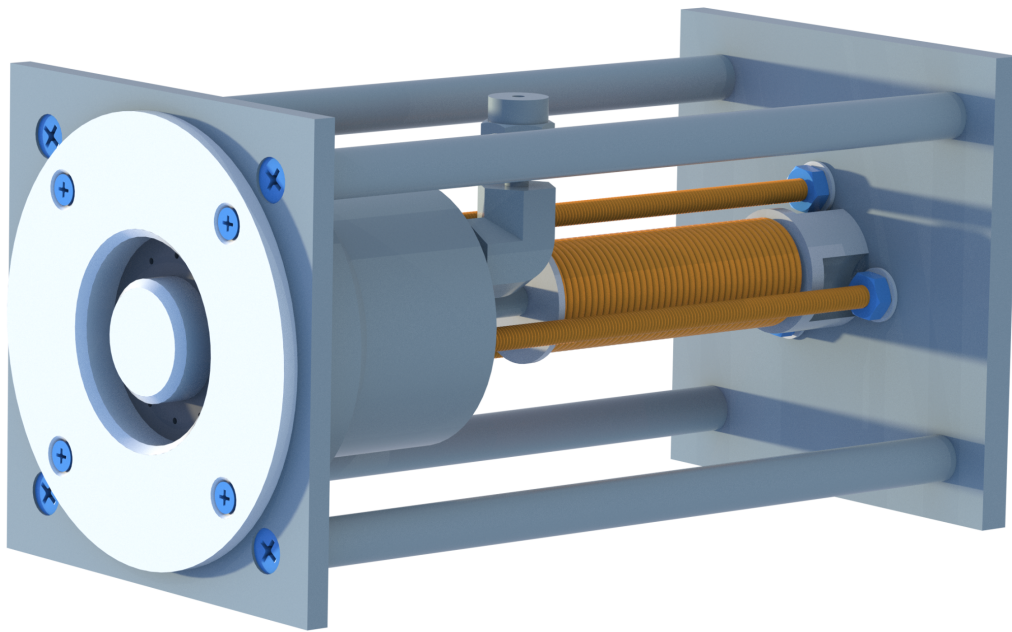
Figure 3.30: Front view of the assembled Hall Thruster
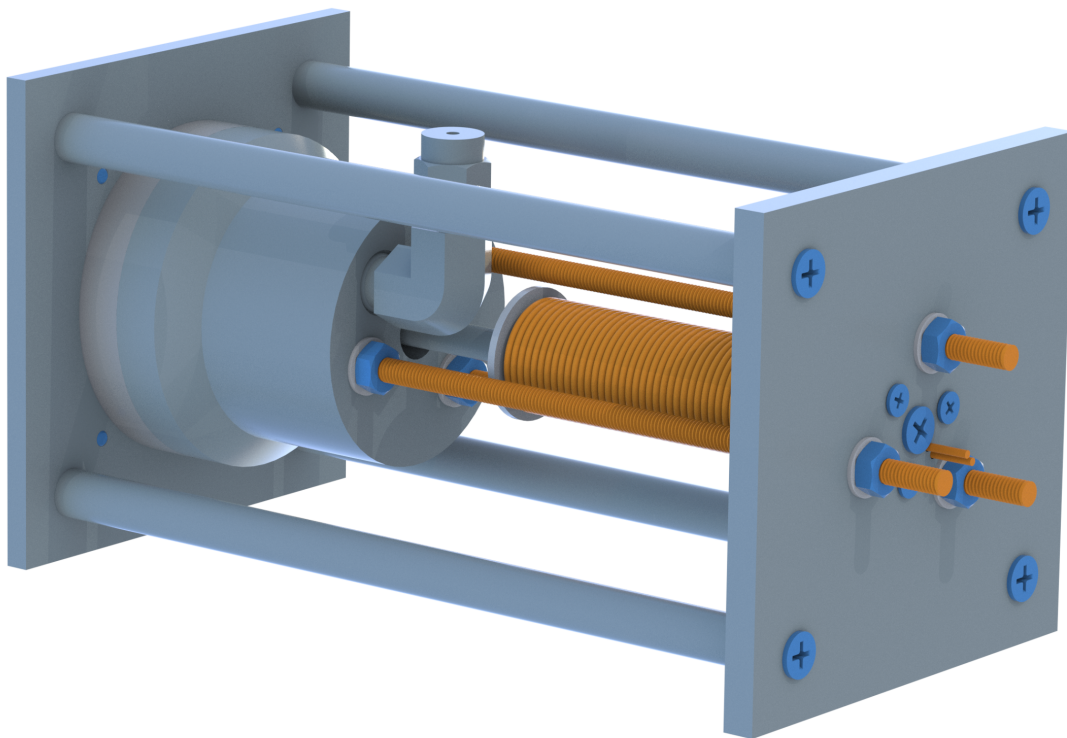
Figure 3.31: Back view of the assembled Hall Thruster

3.7.1 Thruster Specification
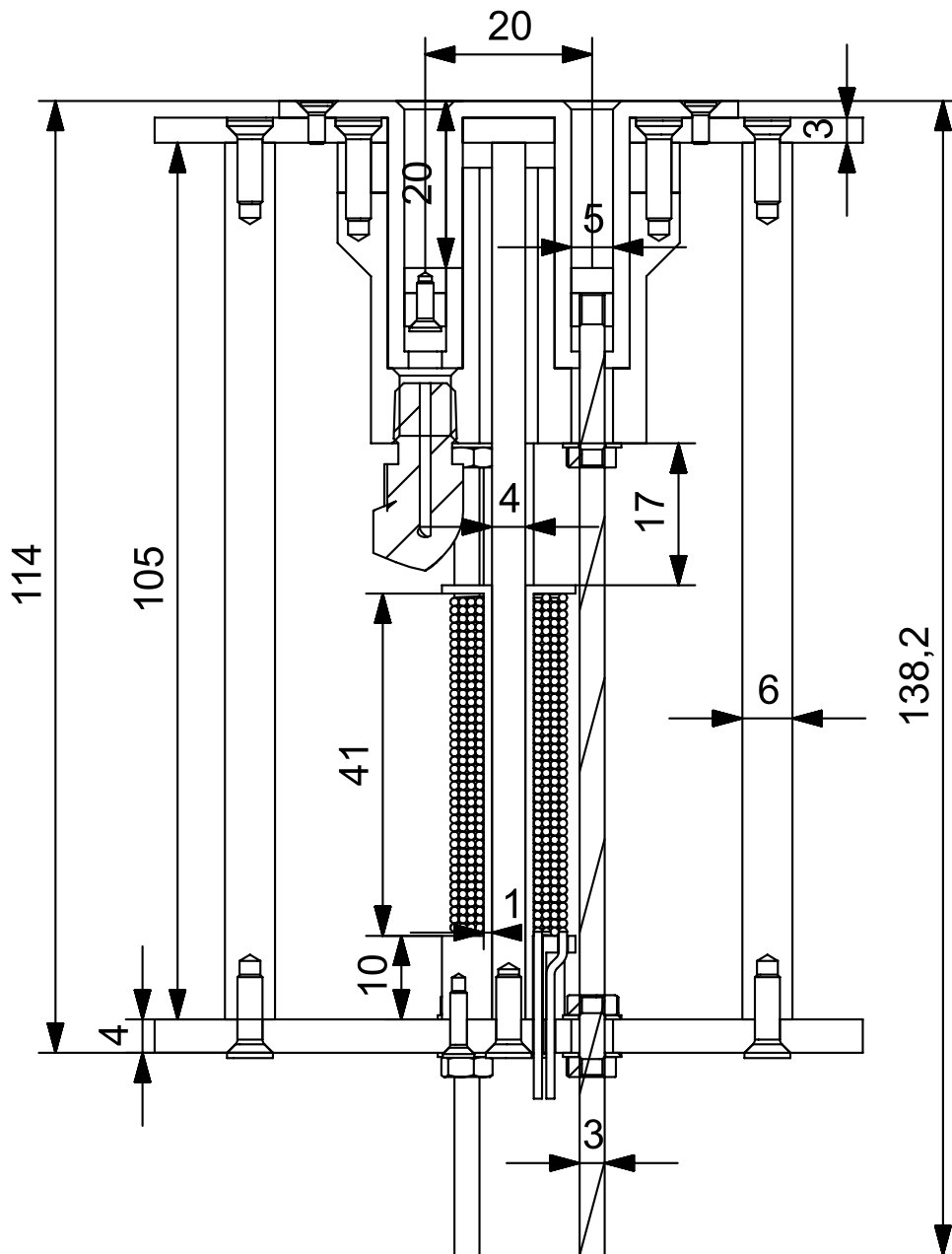
Figure 3.32: Technical drawing of the assembled Hall Thruster in a diagonal cross section

property	symbol	unit	designed Hall Thruster
assembly length		mm	118.2 .. 138.2
assembly width		mm	60
assembly height		mm	60
mass	m	kg	0.524
channel height	h	mm	5
channel diameter	d	mm	20
channel length	L	mm	0..20

Table 3.11: Geometric Parameters of the designed Hall Thruster

quantity	description	material	magnetic	manufacture
1	ceramic discharge channel	BNSiO2 Grade M26 [3]	no	yes
4	DIN 7500 ME-M2x5	Steel	no	no
1	body top plate	1006 Steel (1.0313)	yes	yes
1	body center piece	1006 Steel (1.0313)	yes	yes
1	body bottom plate	1006 Steel (1.0313)	yes	yes
4	body outer pole	1006 Steel (1.0313)	yes	yes
1	body spacer	316 Steel (1.4401)	no	yes
1	body inner pole	Supermalloy	yes	yes
4	DIN 7500 ME-M3x12	Steel	no	no
9	DIN 7500 ME-M3x10	Steel	yes	no
1	anode face plate	Tungsten	no	yes
1	anode body	Copper	no	yes
3	anode threaded rod	Copper	no	yes
3	DIN 7500 ME-M2x6	Steel	no	no
6	ISO 4034-M3	Steel	no	no
3	ZAGO M3 hex sealing nut [30]	Steel, PTFE	no	no
9	DIN125 M3 [35]	PTFE	no	no
1	Fitok SS-LM-FL1-NS1 [7]	Steel	no	no
1	coil case	Aluminium	no	yes
1	IEC 60317-13 wire 1mm	Copper	no	no
3	DIN 7500 ME-M2x8	Steel	no	no

Table 3.12: Parts list of the designed Hall Thruster with properties of requiring manufacturing or not

3.7.2 Estimated Performance

	variable	symbol	value	unit
setting	discharge voltage	U	450	V
	anode mass flow	$\dot{m}_a$	0.770	mg/s
	coil current	I_{coil}	5.5	A
	channel length	L	13	mm
measurement	coil voltage	U_{coil}	<1.06	V
	magnetic flux	B	0.06	T
	discharge current	I_d	2.22	A
	discharge power	P	1000	W
	specific impulse	I_{sp}	1864	s
	thrust	T	14.1	mN
	thrust efficiency	η_T	10.4	

Table 3.13: Design settings and expected performance of the designed Hall Thruster

4 Experimental Setup

Cathode

The hollow cathode was not designed in this work and either has to be developed separately or can be bought as commercial of the shelf component from manufacturers like Electric Propulsion Laboratory, Inc. [17]. They require a separate gas feed with a mass flow controller, as well as further electric power supplies to set their internal potentials.

Vacuum Chamber

In order to conduct actual operation, a vacuum facility is needed. One reference on the vacuum facility pressures are 0.0078 Pa ($78 \cdot 10^{-6}$ mbar) to 0.00033 Pa ($3.3 \cdot 10^{-6}$ mbar) from the SPT-100 tests [5]. Where next to another pressure reference of 10^{-5} mbar to 10^{-9} mbar, the ESA Propulsion Laboratory (EPL) can be taken as reference for pump configurations and chamber sizes [36].

Gas Feed-system

In order to supply a specific mass flow to the thruster, a gas feed system is required. If not directly supplied by an Electrolyzer, it would be supplied by a high pressure storage tank with pressure reducers and mass flow controllers. If a different gas is used for the cathode mass flow, which will be the case in WEP, a parallel feed system has to be established.

Plasma Diagnostics

Next to the electrical power supplies and mass flow controllers, Faraday cups and Langmuir probes can be used to determine electron temperature, electron density, floating- and plasma-potential. In order to gain insight on which side reactions are how frequent, spectroscopy could be deployed, under which the emitting wavelength can be correlated with a known energy release from a certain reaction.

Thrust Balance

As thrust balances on the range of mN are required, a thrust balance similar to the Imperial Collage of London could be constructed, which features an uncertainty of ± 0.1 mN with a range of 1-600 mN, which is based on a modified commercial load–cell [36] [27].

Electrical Equipment

Next to low voltage power supplies for the coil and the thermionic emission of the cathode, a high voltage power-supply suitable for the high power oscillations of the breathing mode needs to be selected.

4.1 Road Map

As this work covered the initial research and design phase in the following road map, the follow-up step should be a revision of the design and a progression into the next major category of the component development already. If however the hollow cathode or the thrust balance is preferred to be developed in house, additional designing has to be performed first or in parallel. Hereby should be mentioned that both of these developments are challenging and time intensive.

Research and Design

- <u>Literature Review</u>: Study existing Hall effect thruster designs, focusing on propellant characteristics, typical operational values, and scaling laws. Identify differences on operation of Oxygen versus Xenon. Understand underlying physical principles to a degree that the chain of events on the plasma can be comprehended.

- <u>Conceptual Design</u>: Create a detailed design of the Hall effect thruster, considering selected power requirements and propellant type.
  Subsystems:

  - Discharge Channel

  - Magnetic Assembly: Core, Coils, Shielding

  - Electrode Assembly: Hallow Cathode, Impact resistant Anode

  - Propellant Management: Injection Interface, Flow Controller (Propellant- and Cathode protection gas)

- <u>Simulation</u>: Utilize simulation software to model key aspects as the general thrust performance, magnetic configuration and plasma behavior.

Component Development

- <u>Magnetic Assembly</u>: Build the magnetic-core, -coils and -shielding elements that generate the specific magnetic field for electron trapping.

- <u>Electrode Assembly</u>: Manufacture the hallow cathode emitter and highly resistant anode.

- <u>Discharge Channel</u>: Manufacture ceramic chamber wall suitable to the chosen propellant.

- <u>Propellant Management</u>: Manufacture injection interface.

- <u>Equipment Selection</u>:

  - Operational Equipment (High- and low voltage power supplies, Flow Controller, Cathode Emitter, Gas storage, Vacuum Chamber)

    − Sensory Equipment (Multimeter, Magnetometer, Magnetic field indicator film, Thrust Measurement Balance, Spectrometer, Langmuir Probe)

Assembly and Pre-Testing

- <u>Thruster Assembly</u>: Assemble the manufactured components of subsystems into a Hall thruster prototype.

- <u>Ground Testing</u>: Perform initial tests to assess the static subsystems functionality. Associate electrical settings with measured magnetic field variables as operating points and confirmation of simulation. Validate the gas flow control.

- <u>Rough Vacuum Testing</u>: Perform hallow cathode emitter tests to assess the subsystems's functionality, efficiency and operating point association.

Testing and Optimization

- <u>Thrust Measurement</u>: Implement and calibrate a thrust measurement system to accurately quantify the thrust output.

- <u>Plasma Diagnostics</u>: Integrate diagnostic tools to measure plasma properties as ion velocity, density, energy distribution and ionisation side products.

- <u>High Vacuum Testbench Assembly</u>: Integrate the full propulsion system in a high vacuum test facility for operational tests.

- <u>Optimize Operational Parameter Space</u>: Sweeping across operating ranges of key variables while holding others constant for sensitivities and keeping others variable for correlations. Providing parameter space.

- <u>Impurity Analysis</u>: Repeat sensitivity tests with impurities to verify dependencies.

- <u>Electrolyseur Coupling</u>: Direct feeding from water electrolysis products. Demonstration of full electric water propulsion system.

5 Conclusion

A design of a Hall Thruster turned out to be complex, not due to its components, but its physics under operation, as there are still many plasma physical relationships to be unraveled that did not receive a mention in this work.

The implementation of the anodes step-less incrementation was a success, which to my personal knowledge is the first thruster to have a continuous adjustable channel length. This feature is the perfect setup to identify the dependency between B to L for Oxygen, as both variables can be set continuously.

Areas to expand on would be, to provide an estimation on temperatures under operation to validate the chosen materials and setup. Also, the angled NPT gas inlet could be a problem for not being able to achieve a 100 % seal, as it is only hardly controllable under which orientation it comes to a stop. One solution could be to mount the connector straight from the side of the thruster, which requires the center piece to be adapted.

One fall back mechanism is the copper coil, which delivers under its designed 5.5 A a very high 0.06 Tesla, while other Hall Thruster operate on much lower magnetic field strengths. This results in the thruster being funcional also with a lower B field, as with 2 A of current 0.03 Tesla could be achieved, which is still more than the thruster used at University Tokyo, which hat 0.014 Tesla. This way the magnetic capabilities are rather strong and versatile in this configuration, which is only possible due to the small gap size and chosen materials.

If moved away from a prototype, or the general magnetic body is well understood, or a 3D magnetic simulation is done, the rearrangement to move the coil to the outer poles would improve the thruster in multiple aspects. When moved away from the center, the coils are experiencing less heat exposure and the thruster length would be drastically reduced. Especially when the optimal channel length has been found, a new version should be compactified.

The selected design voltage of 450 V is really high and likely to overshoot, however this would provide a point of data on how much is too much for Oxygen as propellant. The designed thruster can be still used to identify its optimal combination of voltage and mass-flow under its geometry for the given power point, which in the worst case will only under-perform in efficiency. A comparable power point to other thrusters would be then, what is key to evaluate failures or improvements to the reference thruster.

Bibliography

[1]   Andrenucci, M.; Biagioni, L.; Marcuccio, S.; Paganucci, F.: Fundamental scaling laws for electric propulsion concepts. In: 28th International Electric Propulsion Conference, 2003.

[2]   Azevedo, E. R.; Jones-Tett, K.; Larsen, H.; Reeve, S.; Longhi, E.; Tejeda, J. M.; Moloney, R.; Schwertheim, A.; Knoll, A.: Sizing and preliminary design of a 2-kW water propelled Hall effect thruster. In: Internaltional Electric Propulsion Conference, 2022.

[3]   Boron Nitride Solids - Product Data Datasheet - Saint-Gobain, `https://www.bn.saint-gobain.com/sites/hps-mac3-cma-boron-nitride/files/2022-06/combat-bn-solids-ds.pdf` (accessed 2024-03-03), 2024.

[4]   Boron Nitride Solids - Technical Bulletin - Saint-Gobain, `https://www.bn.saint-gobain.com/sites/hps-mac3-cma-boron-nitride/files/2022-06/combat-bn-solids-machining-tb.pdf` (accessed 2024-03-03), 2024.

[5]   Brophy, J. R.: Stationary plasma thruster evaluation in Russia, 1992.

[6]   Dannenmayer, K.; Mazouffre, S.: Elementary Scaling Relations for Hall Effect Thrusters. Journal of Propulsion and Power, Vol. 27, No. 1, pp. 236–245, Jan. 2011.

[7]   Elbow Tube Fitting - SS-LM-FL1-NS1 - Fitok, `https://www.fitokgroup.com/products-detail/i-6616.html` (accessed 2024-03-03), 2024.

[8]   Electric Propulsion current and future trends - J. A. Gonzalez del Amo - ESA Satcom Final Presentation Days, `https://www.epic-src.eu/wp-content/uploads/Electric-Propulsion-Current-and-Future-Trends-ESA-Satcom.pdf` (accessed 2024-03-03), 2024.

[9]   Esteves, B.; Drag, C.; Bourdon, A.; Alvarez-Laguna, A.: Experimental and numerical investigation of a gridded ion thruster running with different propellants (I2, Xe, Kr, Ar). In: International Electric Propulsion Conference, Massachusetts Institute o f Technology, Cambridge, MA, USA, 2022.

[10] Finite Element Method Magnetics (FEMM) - Magnetostatic Simulation Software, `https://www.femm.info/wiki/HomePage` (accessed 2024-03-03), 2024.

[11] Goebel, D. M.; Katz, I.: Fundamentals of electric propulsion, Jet Propulsion Laboratory - NASA, 2008.

[12] Hall, S. J.; Jorns, B. A.; Cusson, S. E.; Gallimore, A. D.; Kamhawi, H.; Peterson, P. Y.; Haag, T. W.; Mackey, J. A.; Baird, M. J.; Gilland, J. H.: Performance and high-speed characterization of a 100-kW nested Hall thruster. Journal of Propulsion and Power, Vol. 38, No. 1, pp. 40–50, 2022.

[13] Heizmann, S.; Herbertz, A.; Saryczew, J.; Manfletti, C.: Investigation of a Cathode-Vapor-Feed Electrolyser for a Water Electrolysis Propulsion System, 2023.

[14] Herdrich, G.; Bauder, U.; Boxberger, A.; Gabrielli, R.; Lau, M.; Petkow, D.; Pfeiffer, M.; Syring, C.; Fasoulas, S.: Advanced plasma (propulsion) concepts at IRS. Vacuum, Vol. 88, pp. 36–41, 2013.

[15] HETMAn: Hall Effect Thruster Modeling and Analysis - User manual for HETMAn v1.0, 2011.

[16] Hofer, R.; Lobbia, R.; Chaplin, V.; Ortega, A. L.; Mikellides, I.; Polk, J.; Kamhawi, H.; Frieman, J.; Huang, W.; Peterson, P., et al.: Completing the development of the 12.5 kW Hall effect rocket with magnetic shielding (HERMeS). In: 36th International Electric Propulsion Conference, 2019.

[17] Hollow Cathode Plasma Electron Emitters and Systems - Electric Propulsion Laboratory, Inc. (EPL), `https://electricpropulsionlab.com/hollow-cathodes/` (accessed 2024-03-03), 2024.

[18] Koppel, C.; Marchandise, F.; Estublier, D.; Jolivet, L.: The SMART-1 electric propulsion subsystem in flight experience. In: 40th AIAA/ASME/SAE/ASEE Joint Propulsion Conference and Exhibit, 2004.

[19] Lee, E.; Kim, Y.; Lee, H.; Kim, H.; Doh, G.; Lee, D.; Choe, W.: Scaling Approach for Sub-Kilowatt Hall-Effect Thrusters. Journal of Propulsion and Power, Vol. 35, No. 6, pp. 1073–1079, Nov. 2019.

[20] Leiter, H.; Killinger, R.; Boss, M.; Braeg, R.; Gollor, M.; Weis, S.; Feili, D.; Tartz, M.; Neumann, H.; Cara, D. M. di: RIT-μX-high precision micro ion propulsion system based on RF-technology. In: 43rd AIAA/ASME/SAE/ASEE Joint Propulsion Conference & Exhibit, 2007.

[21] Liang, R.: The Combination of Two Concentric Discharge Channels into a Nested Hall-Effect Thruster. PhD thesis, 2013.

[22] Marks, T.; Schedler, P.; Jorns, B.: HallThruster.jl: a Julia package for 1D Hall thruster discharge simulation. Journal of Open Source Software, Vol. 8, No. 86, p. 4672, June 2023.

[23] Munro-O'Brien, T. F.; Ryan, C. N.: Performance of a low power Hall effect thruster with several gaseous propellants. Acta Astronautica, Vol. 206, pp. 257–273, May 2023.

[24] Nakagawa, T.; Yamamoto, N.; Komurasaki, K.; Arakawa, Y.: Experimental Investigation of a Hall Thruster Using Oxygen as the Propellant. JOURNAL OF THE JAPAN SOCIETY FOR AERONAUTICAL AND SPACE SCIENCES, Vol. 51, No. 598, pp. 606–612, 2003.

[25] Safran Spacecraft Propulsion - PPS1350 - Datasheet, `https://www.safran-group.com/sites/default/files/2022-09/PPS1350%20-%20Safran%20Spacecraft%20Propulsion%20-%20Datasheet.pdf` (accessed 2024-03-03), 2022.

[26] Schönherr, T.; Little, B.; Krejci, D.; Reissner, A.; Seifert, B.: Development, production, and testing of the IFM nano FEEP thruster. In: 36th International Electric Propulsion Conference, 2019.

[27] Schwertheim, A.; Rosati Azevedo, E.; Liu, G.; Bosch Borràs, E.; Bianchi, L.; Knoll, A.: Interlaboratory validation of a hanging pendulum thrust balance for electric propulsion testing. Review of Scientific Instruments, Vol. 92, No. 3, Mar. 2021.

[28] Schwertheim, A.; Knoll, A.: Experimental investigation of a water electrolysis Hall effect thruster. Acta Astronautica, Vol. 193, pp. 607–618, Apr. 2022.

[29] Schwertheim, A.; Knoll, A.: Low power thrust measurements of the water electrolysis Hall effect thruster. CEAS Space Journal, Vol. 14, No. 1, pp. 3–17, Mar. 2021.

[30] Sechskant-Dichtungsmutter: Metrisch, M3, Kohlenstoffstahl, Teflon - ZAGO, `https://dichtschraube.com/produkte/dichtungsmuttern/sechskant/` (accessed 2024-03-03), 2024.

[31]   Snyder, J. S.; Chaplin, V. H.; Goebel, D. M.; Hofer, R. R.; Lopez Ortega, A.; Mikellides, I. G.; Kerl, T.; Lenguito, G.; Aghazadeh, F.; Johnson, I.: Electric propulsion for the Psyche mission: Development activities and status. In: AIAA Propulsion and Energy 2020 Forum, 2020.

[32]   Starlink 1010, NASA Space Science Data Coordinated Archive, `https://nssdc.gsfc.nasa.gov/nmc/spacecraft/display.action?id=2019-074D` (accessed 2024-03-03), 2019.

[33]   Taploo, A.; Lin, L.; Keidar, M.: Air ionization in self-neutralizing air-breathing plasma thruster. Journal of Electric Propulsion, Vol. 1, No. 1, p. 25, 2022.

[34]   Tejeda, J.; Knoll, A.: An oxygen-fuelled Hall Effect Thruster: Channel length, ceramic walls and anode material experimental analyses. Acta Astronautica, Vol. 203, pp. 268–279, Feb. 2023.

[35]   Unterlegscheibe (DIN 125) aus PTFE - Reichelt Chemietechnik GmbH + Co. `https://www.rct-online.de/de/befestigungselemente/scheiben-und-ringe/unterlegscheibe-din-125-aus-ptfe` (accessed 2024-03-03), 2024.

[36]   Vacuum Facilities at the ESA Propulsion Laboratory (EPL) - ESTEC, `https://technology.esa.int/lab/tec-m-epl-esa-propulsion-laboratory` (accessed 2024-03-03), 2024.